AN ABSTRACT OF THE THESIS OF

Kyle Clocker for the degree of Master of Science in Electrical and Computer Engineering presented on May 24, 2018.

Title: CMOS-Integrated Single-Element Thermal Flow Sensors

Abstract approved: ______________________________________

Matthew L. Johnston

Flow rate sensors for *in situ* gas or liquid monitoring typically comprise multiple transducer elements, including a heater and one or more temperature sensors to measure the rate of heat energy removal by the flowing fluid. The need for multiple transducer elements limits feasibility of shrinking these sensors to microfluidic flow channels and their integration into standard CMOS processes. In this work, a thermal flow sensor architecture is presented, which is integrated into a CMOS IC without additional post-processing. The architecture uses a single, resistive transducer element to measure fluid flow with a two-phase control and measurement algorithm. Experimental results demonstrate feasibility of the flow sensor architecture using a discrete micron-scale resistor structure, and using an integrated resistor structure for measuring air flow. By separating heating and temperature measurement in time, instead of in space, this method significantly decreases required transducer area and allows for the architecture to be scaled down to an integrated CMOS thermal flow sensor.

©Copyright by Kyle Clocker
May 24, 2018
All Rights Reserved

CMOS-Integrated Single-Element Thermal Flow Sensors

by

Kyle Clocker

A THESIS

submitted to

Oregon State University

in partial fulfillment of
the requirements for the
degree of

Master of Science

Presented May 24, 2018
Commencement June 2018

Master of Science thesis of Kyle Clocker presented on May 24, 2018.

APPROVED:

Major Professor, representing Electrical and Computer Engineering

---

Director of the School of Electrical Engineering and Computer Science

---

Dean of the Graduate School

I understand that my thesis will become part of the permanent collection of Oregon State University libraries. My signature below authorizes release of my thesis to any reader upon request.

Kyle Clocker, Author

ACKNOWLEDGEMENTS

I would like to acknowledge the Starting State and the Transition Function.

TABLE OF CONTENTS

Page

1 Introduction 1

1.1 Operating Principle of Thermal Flow Sensors 1

1.2 Traditional Flow Sensor Architectures 2

1.2.1 Hot-Wire/Film Thermal Flow Sensors 2

1.2.2 Calorimetric Flow Sensors 2

1.2.3 Time of Flight Sensors 4

1.3 Delta-Sigma Thermal Flow Sensors 4

1.4 Flow Sensing Elements 7

2 Review of Chip-Scale Flow Sensors 9

2.1 MEMS Thermal Flow Sensors 9

2.2 CMOS-Integrated Thermal Flow Sensors 10

2.3 New Thermal Flow Sensing Architectures 12

2.3.1 An Electrochemical Impedance-Based Thermal Flow Sensor for Physiological Fluids 12

2.3.2 A Chip-Integrated Highly Variable Thermal Flow Rate Sensor . . 14

3 Dual-Slope Single-Element Thermal Flow Sensor 18

3.1 Single-Element Flow Sensor Architecture 18

3.2 Dual-Slope Control Methods 19

3.2.1 Dual-Slope ADC 19

3.2.2 Dual-Slope Flow Measurement 20

3.3 Discrete Single-Element Flow Sensor System Design 22

3.3.1 Constant-Power Regulator Circuit 22

3.3.2 Resistance Measurement Circuit 25

3.3.3 FPGA-Based Dual-Slope Sensor Control 25

3.4 Resistive Sensor Element 27

3.4.1 Sensor Element Design Considerations 27

3.4.2 Sensor Element Design and Fabrication 29

3.4.3 Sensor Element Thermal Characterization 31

3.5 Discrete Dual-Slope Flow Sensor Testing 32

3.5.1 Experimental Setup 32

3.5.2 Variable Flow Rate Measurement Results 32

3.5.3 Variable Heating Time Measurement Results 33

TABLE OF CONTENTS (Continued)

Page

3.6 Metered Flow Sensor Tests . . . 33

3.6.1 Experimental Test Setup . . . 35

3.6.2 Variable Flow Rate Measurement Results . . . 35

3.6.3 Variable Heating Time Measurement Results . . . 39

4 CMOS Single-Element $\Delta\Sigma$ Thermal Flow Sensor 42

4.1 Single-Element Thermal $\Delta\Sigma$ Flow Sensor . . . 42

4.2 Circuit and Element Design . . . 43

4.2.1 Top-Level System Design . . . 44

4.2.2 Thermometer-Encoded Current Source Design . . . 45

4.2.3 DC Level Boosting Circuit . . . 47

4.2.4 Comparator Design . . . 47

4.2.5 Element Design . . . 47

4.2.6 Flow Sensor IC Fabrication . . . 51

4.3 Test Setup . . . 52

4.4 Experiments and Results . . . 52

4.4.1 Element Characterization . . . 52

4.4.2 Flow Measurement . . . 54

4.4.3 Effect of SiO_2 Passivation on Sensor Element . . . 57

4.4.4 Discussion . . . 57

5 Conclusion and Future Work 59

5.1 Conclusions . . . 59

5.2 Future Work . . . 60

Bibliography 60

LIST OF FIGURES

Figure | Page

1.1 (a) Structure of hot-wire thermal flow sensor from [19]. (b) Output from hot wire thermal flow sensor from [19]. 3

1.2 (a) Heat profile change due to flow onto a calorimetric flow sensor from [1]. (b) Example of a calorimetric flow sensor output. The output is the temperature difference between the two sensors illustrated in Fig. 1.2a [1] 5

1.3 Example of a time of flight flow sensor configuration from [9]. The heater element generates heat pluses and the flow pushes them down to the temperature measurement element separated by a distance X_m. 6

1.4 Example of two different temperature outputs from the time of flight flow sensor presented in [9]. A zero flow, $\Phi = 0$, case is shown by t_1, and a higher flow case, $\Phi > 0$, is shown by t_2. 6

1.5 (a) Block diagram of a typical thermal $\Delta\Sigma$ system. (b) Timing diagram of a typical thermal $\Delta\Sigma$ system. 8

2.1 Fabricated double heater thermal flow sensor shown in [18]. A microscope image of the double heater is shown in (a), the sensor in channel in (b), and entire assembly in (c). 10

2.2 Output voltage from the double heater thermal flow sensor shown in [18]. Output voltage is from a Wheatstone bridge measuring the resistance difference in the two elements as flow increases. 11

2.3 (a) Fabrication process for CMOS thermal flow sensor presented in [11]. (b) Die photo of diode-based CMOS thermal flow sensor from [11]. 13

2.4 Comparison of diode thermal flow sensor to thermoresistive thermal flow sensor. The diode base version has a higher output due to the greater sensitivity of the diodes and co-location by heating elements. 14

2.5 (a) Flow bringing heat across the impedance sensor. As the fluid heats up the impedance of the fluid changes. The flow brings heat from the heater across the sensor [2]. (b) Picture of the sensing structure fabricated on a thin flexible film. 15

LIST OF FIGURES (Continued)

Figure | Page

2.6 (a) Measurement of impedance change in fluid as heater is turned on and off [2]. (b) Experimental results showing full range and sensitivity of the thermal flow sensor. 15

2.7 (a) Photo of the process and fabricated luminescent thermal flow sensor [6]. (A) shows and exploded view of the flow sensor, (b) a cross sectional view and (c) a photo of the fabricated sensor. (b) Data from a thermal flow sensing experiment. A shows a false colored temperature scan of the two regions of interest (ROI), (b) shows temperature measurements from each ROI with flow rate and (c) shows the temperature difference between the two ROI across flow rate. 17

3.1 Thermal-electrical model of single-element flow sensor. A resistive element is actively heated and passively cooled, and its change in resistance is used to measure flow rate over the element. 19

3.2 Dual-slope timing diagram 21

3.3 A block diagram of the top level of the discrete single-element flow sensor PCB. 23

3.4 Photograph of the completed test PCB used to test the dual-slope control algorithm using the single-element thermal flow sensor. 23

3.5 A schematic of the constant power regulation circuit 24

3.6 Block diagram of the FPGA 26

3.7 Diagram of the dual slope measurement state machine. 28

3.8 (a) Layout of the element in Cadence Virtuoso. (b) Microscope image of a section of the manufactured element 30

3.9 Manufactured element's resistance across temperature 31

3.10 Fan-based flow sensor test setup 32

3.11 (a) Measured cooling time (T_m) for the single-element sensor under varying air flow. Arrows indicate sample at which fan speed was changed. (b) Histogram showing the distribution of cooling time (T_m) at each tested fan speed, as an indication of measurement noise and resolution. 34

LIST OF FIGURES (Continued)

Figure | Page

3.12 Flow adjustment valve and meter 36

3.13 Model of the two-part baffle used to smooth out the air flow in the flow chamber. 37

3.14 Picture of the element installed into the metered flow chamber 37

3.15 Dual-slope flow meter demonstration with 1 S heating time. 38

3.16 Warm-up periods for the element at (a) 1 s heating time (b) 100 ms heating time. Flow levels are annotated over their respective regions. 39

3.17 Flow measurement from on-chip element (a) 100 mS heating time, and (b), surface temperature at each system location. Flow levels are annotated over their respective regions. 40

3.18 Flow measurement from on-chip element (a) 200 mS heating time, and (b), surface temperature at each system location. Flow levels are annotated over their respective regions. 41

4.1 Block diagram of the proposed single-element thermal ΔΣ system. 43

4.2 Timing diagram of the proposed single-element thermal ΔΣ system. . . . 44

4.3 Block Diagram of the Flow Sensor Chip. 45

4.4 Schematic and layout of the thermometer encoded current source, (a) schematic (b) layout. 46

4.5 General purpose single stage op-amp used in DC level boosting circuit and as a buffer, (a) schematic (b) layout. 48

4.6 Diode ladder reference voltage generator for the DC level boosting circuit. 49

4.7 (a) Schematic of the op-amp based comparator. (b) Layout of the comparator. 50

4.8 On-chip resistor where each layer change consists of two vias in parallel. This was done to ensure sufficiently high current densities could be supported, while still maintaining a high resistance density. (a) is a 3-D illustration of the structure and (b) is the layout. 51

LIST OF FIGURES (Continued)

Figure | Page

4.9 Die photo of single element flow sensor 52

4.10 The complete setup for the testing of the single-element flow sensor IC installed into the test chamber. 53

4.11 Resistance of the two parallel elements as they heat (red) and cool (blue) 55

4.12 Flow measurement from on-chip element without SiO^2 passivation for (a) 1 mS heating time (b) 100 μS heating time. 56

4.13 Flow measurement from on-chip element (a) with SiO_2 layer (b) without SiO_2 layer. 58

LIST OF TABLES

Table Page

3.1 Different cooling times due to variation of the sensor's heating time 33

Chapter 1: Introduction

Electronic flow sensors are needed in any application that needs to move, measure, control, or act on fluids. One of the first applications of electronic flow sensors were for use in automobiles for electronic mass flow sensors. Since then, flow sensors of all types have been found a multitude of industries: HVAC, industrial automation, consumer products, civil engineering, and medical devices. With advances in integrated circuit technology and microeletromechanical systems (MEMS) manufacturing, flow sensors have been looked to for a reduction in size, operating power, and integration. Recent advances in micro-fludics research require flow sensors that scale for integration into the flow channels. microfluidics research also require modern flow sensors to measure smaller flow rates and to be bio-compatible.

1.1 Operating Principle of Thermal Flow Sensors

Thermal flow sensors attempt to measure flow by using the fluid's flow to exchange heat with the sensor [8]. Typically these sensors have a heater, a temperature measurement element, measurement circuity, and control circuitry. As a operating principle is the heater causes a change in temperature in the system, and as a fluid flows across the heater, heat is conducted away from the heater. This causes a change in temperature around the heater. This change in temperature is measured and is representative of the flow.

Flow sensors operate in two main control modes: constant power mode (CP) or constant temperature differential mode (CTD). In constant power mode, the flow sensor maintains a constant power into its heating element, regardless of the flow. As the flow rate changes, the element's temperature will change. Due to the heating element supplying a constant power, the energy into the system is always fixed, and the fluid flow is the main contribution to energy leaving the system and thus temperature change. Typically for these systems, flow output is a temperature measurement of the heater or location in the flow channel near the heater [15].

Constant temperature differential flow sensors operate by trying to keep either the heater or an area around the heater at a constant temperature above ambient. Typically, the heater's power source is in a control loop with a temperature sensor [15]. As the flow rate increases, the power needed to keep the temperature differential increases, and vice-versa. Typically these systems output a flow measurement of the needed power or a voltage/current across the heating element. This style of flow sensor is typically more immune to ambient temperature changes as most implementations take their temperature differential against the ambient. Also, these flow sensors can be made more linear due to there ability to scale the heating power reaction to the thermal response of the system. Two drawbacks exist with this control method over the CP flow sensors. The first is a higher overheat temperature is typically required out of these systems. As they work to keep the temperature above ambient, this causes local temperatures to typically be much higher than ambient. The higher required temperatures could lead to issues with bio-compatibility and require more power to operate.

1.2 Traditional Flow Sensor Architectures

In practice there are three common flow sensing architectures: hot-wire/hot-film, calorimetric, and time-of-flight thermal flow sensors.

1.2.1 Hot-Wire/Film Thermal Flow Sensors

Hot-wire thermal flow sensors typically have two elements, a heating element and a temperature sensing element down stream from the heating element. An early example from [19] shows a hot wire anemometer, Fig. 1.1a. In this sensor, the heating and sensing elements are platinum resistors in a Wheatstone bridge configuration. A typical output from this style of sensor is a non-linear curve saturating at the higher range of measurable flow rates, shown in Fig. 1.1b.

1.2.2 Calorimetric Flow Sensors

Calorimetric flow sensors measure the change in temperature profile around a heating element due to the change in flow [20, 1]. As the flow rate changes, it pushes the

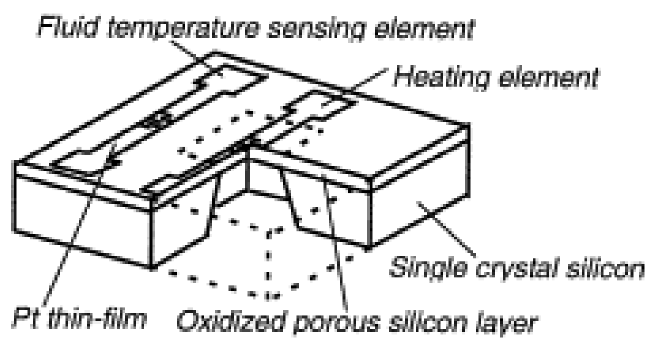

(a)

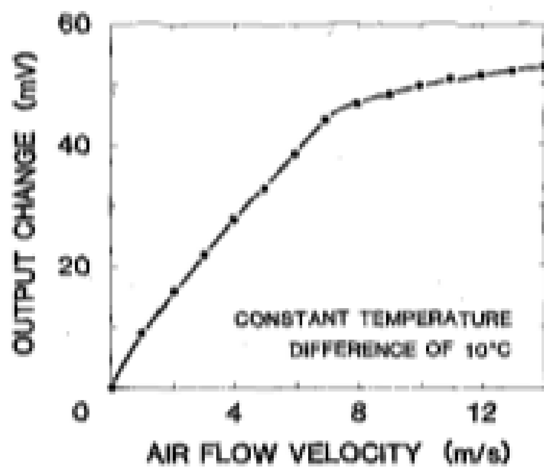

(b)

Figure 1.1: (a) Structure of hot-wire thermal flow sensor from [19]. (b) Output from hot wire thermal flow sensor from [19].

distribution of heat asymmetrically around the heater as shown in Fig. 1.2a. This heat distribution is measured using two or more local temperature sensing devices and this temperature profile is reported as the flow measurement. The calorimetric flow sensor has two different operation regions, the heating region and cooling region. In lower flow situations the flow will push more heat onto one of the temperature sensors and this causes a rise of temperature on that sensor. Eventually the flow will rise too much where it will all be pushed away from the sensor, this is the cooling region of the flow sensor. This style of flow sensor is popular for a couple of reasons, one its naturally immune to ambient temperature changes as it measures a temperature profile around the sensor and the distances are small, and it allows for natural directional flow sensing with its two temperature sensors.

1.2.3 Time of Flight Sensors

Time-of-flight thermal flow sensors measure flow by sending pulses of heat into the flowing fluid. The pulses are carried downstream by the flowing fluid. The sensor uses the time of the pulse along with the pulse shape and measured amplitude to report a flow measurement. As the flow rate rises, the time it takes for the pulses to travel will be reduced. An example, illustrated in [9], has a heating element and a resistive temperature sensor (Fig. 1.3). Heat pulses are generated periodically, and the downstream temperature is a function of both time and flow rate of the fluid. At low or zero flow rates, the measured temperature pulse is of lower amplitude and takes a longer amount of time to appear. In higher flow rates the temperature pulse is of a higher amplitude and arrives more quickly (Fig. 1.4). By looking at the time and amplitude information the flow rate of the fluid can be measured.

[tbph]

1.3 Delta-Sigma Thermal Flow Sensors

Thermal $\Delta\Sigma$ flow sensors are a style of flow sensors that take their operation from the analog-to-digital converters (ADCs) of the same name. Delta-sigma converters use low bit-depth converter and operate at high speed to convert analog signals into a digital pulse stream. They have grown in popularity, in part, due to their simple requirements

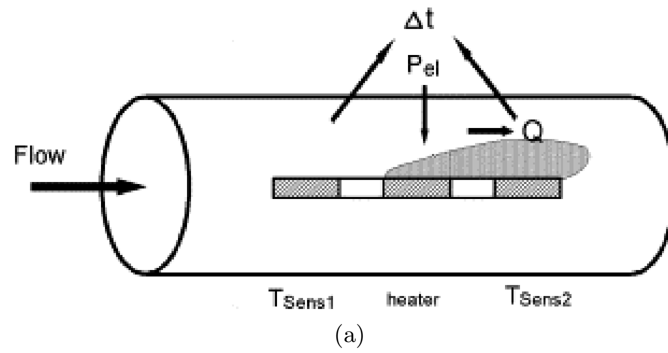

(a)

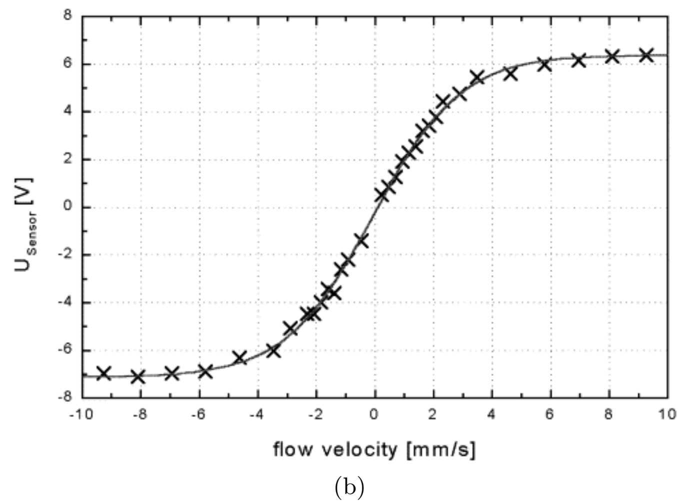

(b)

Figure 1.2: (a) Heat profile change due to flow onto a calorimetric flow sensor from [1]. (b) Example of a calorimetric flow sensor output. The output is the temperature difference between the two sensors illustrated in Fig. 1.2a [1]

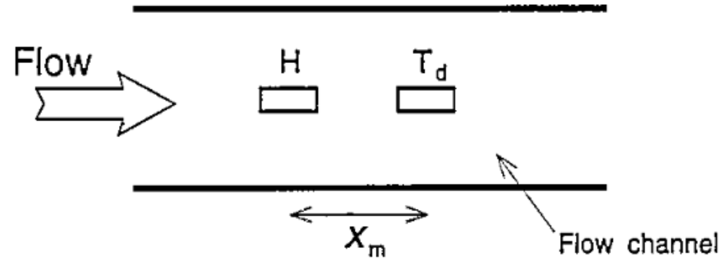

Figure 1.3: Example of a time of flight flow sensor configuration from [9]. The heater element generates heat pluses and the flow pushes them down to the temperature measurement element separated by a distance X_m.

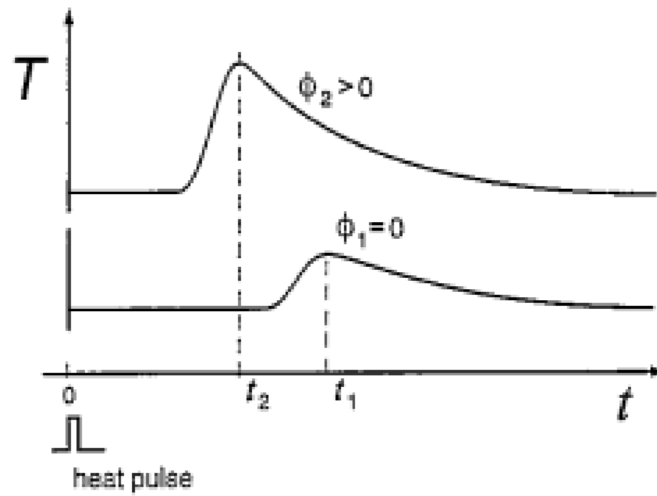

Figure 1.4: Example of two different temperature outputs from the time of flight flow sensor presented in [9]. A zero flow, $\Phi = 0$, case is shown by t_1, and a higher flow case, $\Phi > 0$, is shown by t_2.

for analog components. The low complexity and operation of the converters lends itself well to a thermal adaption [21, 12, 22]. A typical thermal $\Delta\Sigma$ flow sensor, shown in Fig. 1.5a, converts the temperature of an object into a stream of digital pulses. The system attempts to keep the temperature of a sensing element at a steady value by turning the heater on and off. Turning the heater on adds heat to the system, causing the temperature of the element to rise, Fig. 1.5b. When the temperature rises above a reference, the heater is turned off. Heat is continuously conducted away into the ambient environment and by the fluid flowing across the sensing element. As the temperature falls below a threshold, the heater is turned on again. The output of the comparator is fed into a flip-flop, and this pulse stream is used to represent the flow measurement. As the flow rate rises, more heat is required to keep the system above the reference, and the system will cool below the reference more quickly, resulting in more time the heater is on. In lower flow, the heater will be off for a greater part of the time. This is an overall simple scheme, needing only a few simple electronic components: a comparator, flip-flop, heating element, and a temperature transducer. The output of this style of flow sensor is also a digital pulse stream not needing any circuity for integration into a digital system.

1.4 Flow Sensing Elements

In thermal flow sensors, the temperature sensing elements are typically either thermoresistive elements or thermoelectronic elements. Thermoresistive elements are elements that are resistive in nature where resistance changes with temperature. Typically these elements are made of a thin film of a metallic material. They are easy to pattern into needed shapes and a variety of resistances and thus are the most common style of flow sensing elements. Due to the relative ease of patterning metal onto various devices they are typically the easiest to integrate and easier to have direct contact with the measurement fluid. Thermoelectric devices utilize a thermoelectric property of a material to measure temperature. Typically these devices are made in semi-conducting materials and are able to be designed to give a predictable and sensitive response to a change in temperature. The drawback is that the devices are typically more difficult to integrate into a microfluidic system.

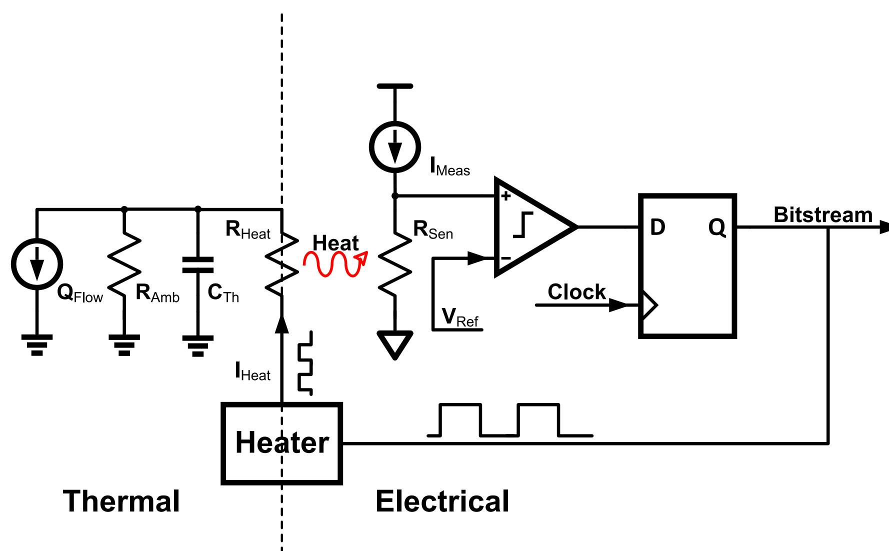

(a)

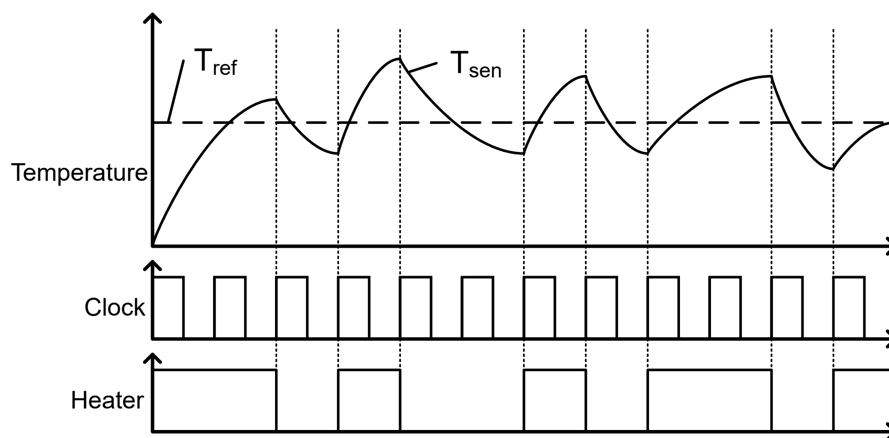

(b)

Figure 1.5: (a) Block diagram of a typical thermal $\Delta\Sigma$ system. (b) Timing diagram of a typical thermal $\Delta\Sigma$ system.

Chapter 2: Review of Chip-Scale Flow Sensors

Modern advances in thermal flow sensors are focused on developing smaller, more integrable sensors for microfluidics applications. As microfluidics fabrication advances the need for smaller integrateable flow sensors has risen. The shrinking volume of flow channels has driven a requirement for flow sensors to be more sensitive to measuring lower flow rates. New MEMS manufacturing techniques are allowing for flow sensors to be placed in-vivo with fluids monitoring. In addition, thermal flow sensors are being adapted for CMOS manufacturing. Finally, other modern advances are developing new thermal flow sensing architectures.

2.1 MEMS Thermal Flow Sensors

A large area of research in thermal flow sensors uses MEMS technology in the design and integration of thermal flow sensors. MEMS manufacturing techniques are enabling sensors to be made smaller and packaged with micro-fluidic channels [14]. These techniques are also being used to design sensors that are used for monitoring of flow in medical applications, such as flow monitoring in micro-needles [10], or sensors designed to be biocompatiable for monitoring breathing [5]. One of the primary design goals for these flow sensors is to be sensitive to low flow rate. MEMS manufacturing techniques allow for the careful design of heating and sensing elements for these low flow applications [23, 4].

Looking at the work presented in [18], the MEMS two heater thermal flow sensor has a double element configuration where each element is both a heater and a temperature sensor. The elements are placed in opposing arms of a Wheatstone bridge, and their resistance difference is measured and amplified to the output. The two sensors are built to the same resistance, thus doubling the output from the Wheatstone bridge compared to single-element version. The sensors are fabricated out of a Cr/Pt deposition process and suspended in a silicon/glass micro-fluidic channel. The researchers simulated the effects of the heater lengths and the distances between the heaters. The simulations

indicated an optimal length of 1.5 mmm and 1.5 mm distance between the heaters. The fully fabricated flow sensor is shown in Fig. 2.1. The flow rate was measured between 0.5 sscm and 10 sscm with steps of 0.5 sscm. from 0-6 sccm the output voltage from the measurement was found to be linear, and deterioration was found in flow rates above 6.0 sscm. The data from this experiment is shown in Fig. 2.2. Another experiment was performed stepping down the flow rate, which provided similar results with a slope of decrease near the same as the increasing slope. From these two tests the derived sensitivity of the sensor is found to be 0.3 mV/mL/min in the lower flow range (0.5-6.0 sscm).

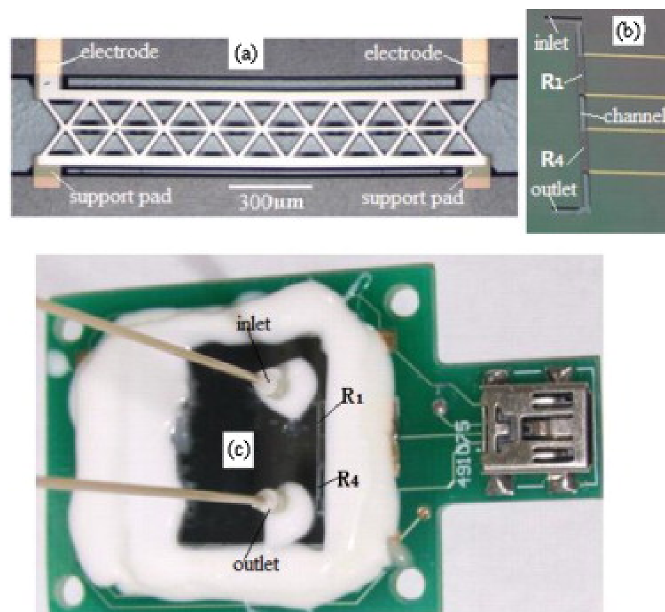

Figure 2.1: Fabricated double heater thermal flow sensor shown in [18]. A microscope image of the double heater is shown in (a), the sensor in channel in (b), and entire assembly in (c).

2.2 CMOS-Integrated Thermal Flow Sensors

Due to CMOS being the pervasive technology for integrated circuits, researchers have been trying to bring thermal flow sensors into CMOS technologies. The ease of manufacturing and integration with control and readout circuitry drive research in this direction.

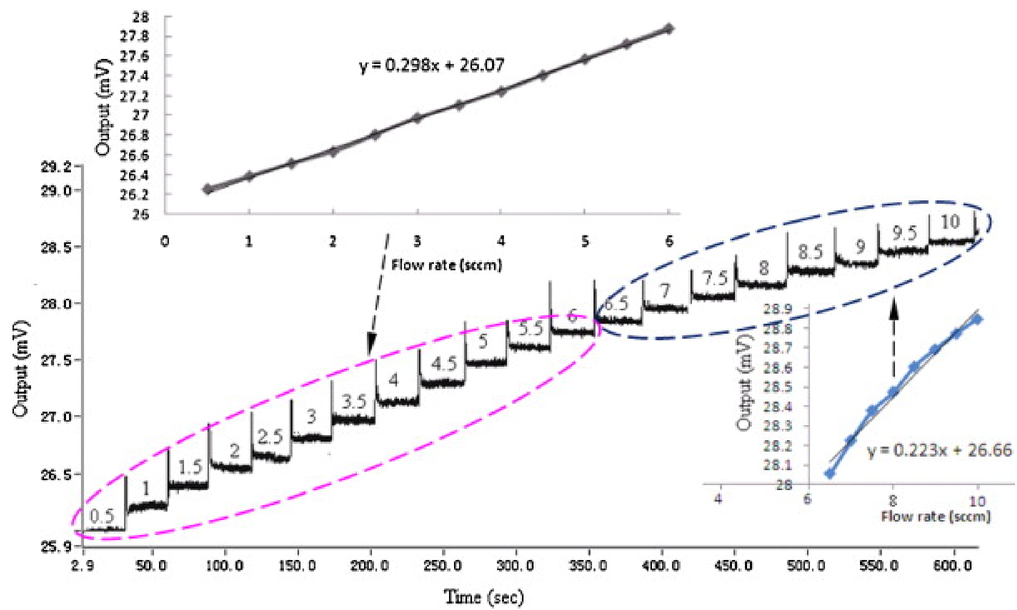

Figure 2.2: Output voltage from the double heater thermal flow sensor shown in [18]. Output voltage is from a Wheatstone bridge measuring the resistance difference in the two elements as flow increases.

Silicon thermopiles are often used for sensing and heating elements [13], typically having a similar response to thermoresistive elements. Another challenge is interfacing the flow sensor to fluid flow. One example uses a flip-chip boding to a thermal exchange disk, [17], while another seals the chip inside the flow channel with sensing elements [24].

In [11], a thermal flow sensor is manufactured on a SOI CMOS process that combines several CMOS integration techniques. The sensing elements are diode arrays, and an additional diode is located under the sensor for heater temperature control. The heater is made using tungsten traces on top of the heater temperature diode. The fabrication of the flow sensor is shown in Fig. 2.3a. By etching a membrane, the sensor has some thermal isolation, which improves the performance of the sensor. The manufactured disk is shown in Fig. 2.3b. The authors report several advantages to using diodes over resistance-based temperature sensors, including better performance, lower power, and lower required area. Also, diodes are straightforward to design and integrate into CMOS processes. The authors tested diode sensitivity to flow measurements compared to a thermoresistive variant and found a 42 % increase, as shown in Fig. 2.4

2.3 New Thermal Flow Sensing Architectures

A majority of thermal flow sensors operate using thermoresistive or thermoeletric materials for heating and temperature sensing, but new methods of flow sensing based on changes in impedance [2] due to heating and thermo-luminescent effects on flowing fluids [6].

2.3.1 An Electrochemical Impedance-Based Thermal Flow Sensor for Physiological Fluids

The research group from [2] presents a new thermal flow sensor for in-vivo applications. The sensor is a time-of-flight architecture measuring the temperature-induced impedance change in a fluid. The theory behind this sensor is that fluids in the body have some electrolytic conductivity, and this conductivity is analogous to the temperature coefficient of resistance of other materials. The heater heats the solution, and the heated fluid is brought across the impedance sensor by the flow as shown in Fig. 2.5a. As the heat diffuses across the sensor, the impedance decreases as shown in Fig. 2.6a. The flow rate

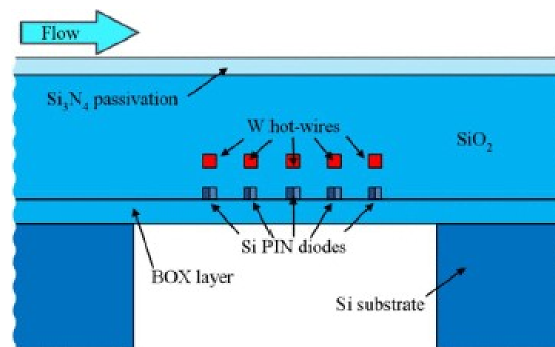

(a)

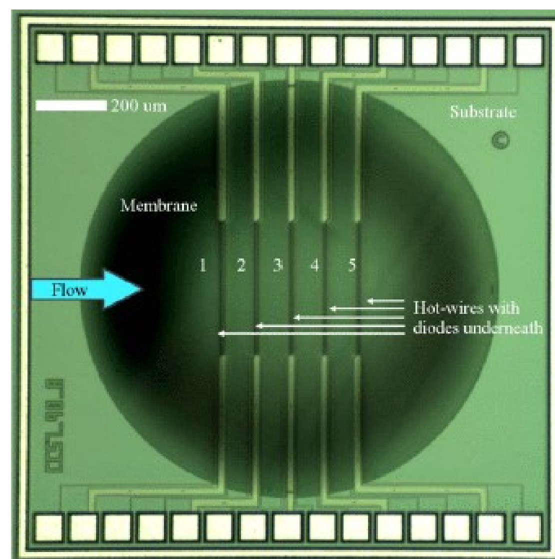

(b)

Figure 2.3: (a) Fabrication process for CMOS thermal flow sensor presented in [11]. (b) Die photo of diode-based CMOS thermal flow sensor from [11].

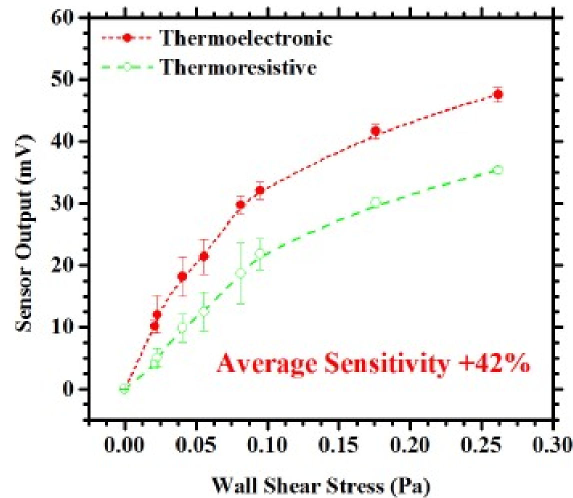

Figure 2.4: Comparison of diode thermal flow sensor to thermoresistive thermal flow sensor. The diode base version has a higher output due to the greater sensitivity of the diodes and co-location by heating elements.

in the channel has an effect on the rate of impedance change in the fluid therefore; the flow measurement is reported back as a maximum change of impedance. As this works on diffusion, a change the flow can be measured in either direction. The sensor was designed on a thin-film substrate with platinum heater element and exposed electrode. The fabricated sensor is shown in Fig. 2.5b. The distance between heater and electrodes were tested, and 1 mm was found to be the optimal point for this design. Overall the sensor was characterized as having a 43.3 μm/s resolution and a range of $\pm$0.8 mm/s flow rate, as shown in Fig. 2.6b

2.3.2 A Chip-Integrated Highly Variable Thermal Flow Rate Sensor

A microfluidic integrated lab-on-chip calorimetric flow sensor is demonstrated in [6]. The flow rate sensor is heated with an on-chip heater, and temperature measurement is done using a luminescent temperature sensing layer in the the fluid channel. The sensor is constructed by first making the micro-fluidic channel on a glass substrate and then coating the walls of the channel with thin polymer layers. Then the chemical sensor is deposited onto the walls. An inkjet printed resistive heating element is deposited onto

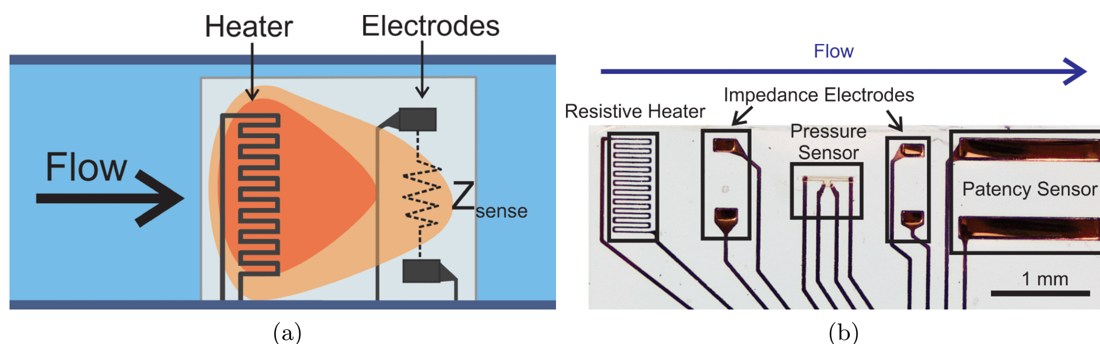

Figure 2.5: (a) Flow bringing heat across the impedance sensor. As the fluid heats up the impedance of the fluid changes. The flow brings heat from the heater across the sensor [2]. (b) Picture of the sensing structure fabricated on a thin flexible film.

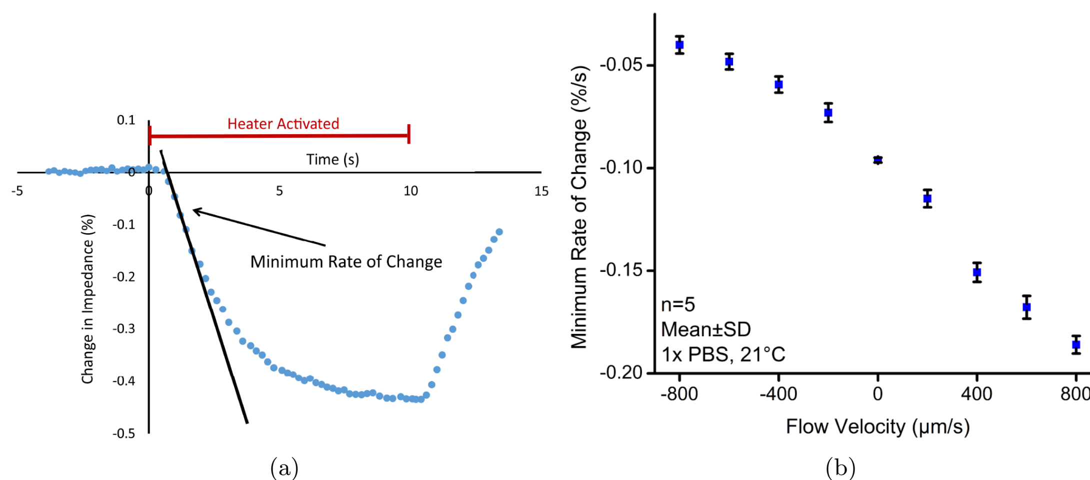

Figure 2.6: (a) Measurement of impedance change in fluid as heater is turned on and off [2]. (b) Experimental results showing full range and sensitivity of the thermal flow sensor.

a PMDS foil, and the PMDS housing sandwiches the foil onto a micro-fluidic channel. This process is illustrated in Fig. 2.7a. The readout of the sensor was done with an external microscope, excited by an external white led. Under zero flow, the channel was read for light intensity across its length, and the calorimetric style curve was seen in the intensity graph. This proof of concept measurement was repeated under a flow condition, and a heat distribution across the channel was shown. To mimic a traditional calorimetric flow sensor, two points were chosen on both sides of the heat sensor to measure sensor response across varying flow rates from, 1 μl/min to 150 μl/min. The data shown in Fig. 2.7b found similar performances to other fully electric flow sensors with a similar amount of power used. With the ability to measure temperature across the entire channel, the sensor has the ability to be tuned to match varying flow rate requirements. This allows for more or less sensitivity depending on the range of flow rates required to be measured. The total range demonstrated was from 10 nL/min to 15 μL/min.

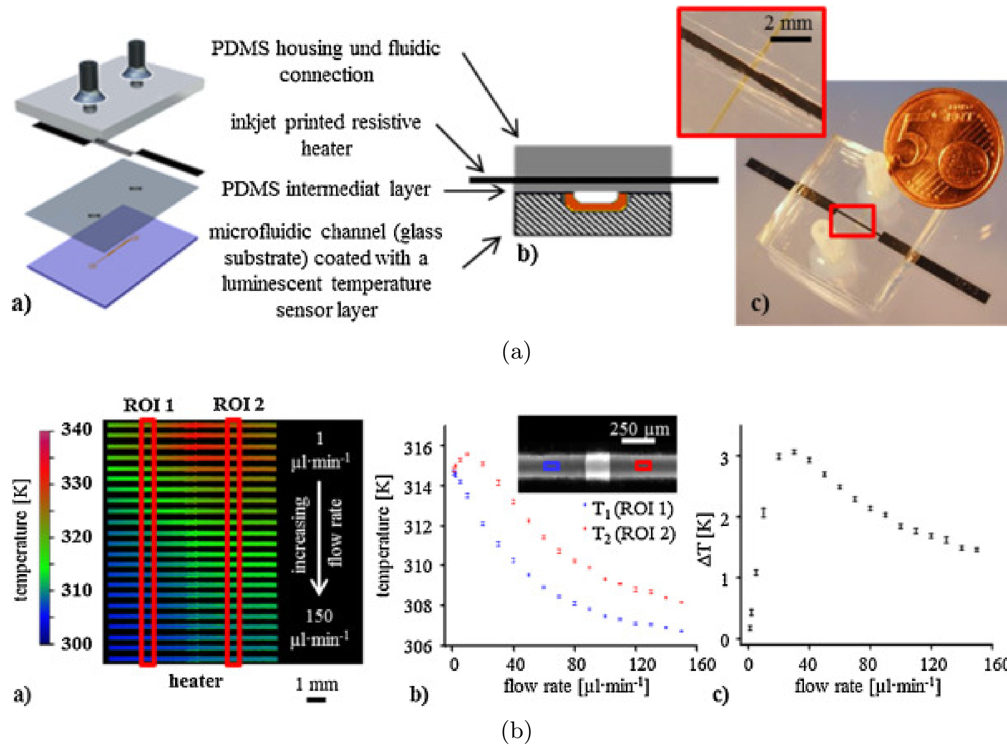

Figure 2.7: (a) Photo of the process and fabricated luminescent thermal flow sensor [6]. (A) shows and exploded view of the flow sensor, (b) a cross sectional view and (c) a photo of the fabricated sensor. (b) Data from a thermal flow sensing experiment. A shows a false colored temperature scan of the two regions of interest (ROI), (b) shows temperature measurements from each ROI with flow rate and (c) shows the temperature difference between the two ROI across flow rate.

Chapter 3: Dual-Slope Single-Element Thermal Flow Sensor

Flow sensor implementations presented in Chapter 2 typically require at least two physical elements, a heater and a temperature sensor. Separating these heating and measurement steps in time, instead of in space, it is instead possible to measure fluid flow using a single transducer element and a two-phase, 'dual-slope' control algorithm. This single-element thermal flow sensor, in which a resistive transducer is used alternately as heater and temperature sensor, simplifies sensor fabrication and is easily scalable to support liquid and gas flow rate sensing on the micron scale. This is of particular value for the development of miniaturized gas sensor systems and lab-on-chip applications.

3.1 Single-Element Flow Sensor Architecture

Flow measurement using a single element requires sharing the element in the time domain. Sensor operation occurs in two phases, where alternate heating and cooling cycles can vary to measure flow. In the heating phase, the element is used as a resistive heater. A current is allowed to flow into the element, and resistive heating heats the element to a temperature above the surrounding ambient temperature. During the cooling phase, the heating current is switched off, and a small measurement current is supplied to the element to measure resistance. The element is allowed to cool, and the resistance is measured as it falls due to cooling; this rate of cooling is a function of fluid flow rate.

The complete system can be modeled as shown in Fig. 3.1. On the thermal side, current sources represent heat sources adding heat into the system. The resistor represents the thermal resistance between the element and the substrate. The nearby substrate acts as a thermal capacitor, sinking and storing heat. The voltage, V_1, represents the temperature of the heater compared to ambient. The heating and cooling of the system is comparable to charging and discharging a capacitor, which gives a nonlinear response for the sensor to the surrounding fluid flow. For constant flow, flow rate can be measured by examining either one or both the heating time or cooling time for a fixed temperature difference in the sensing element.

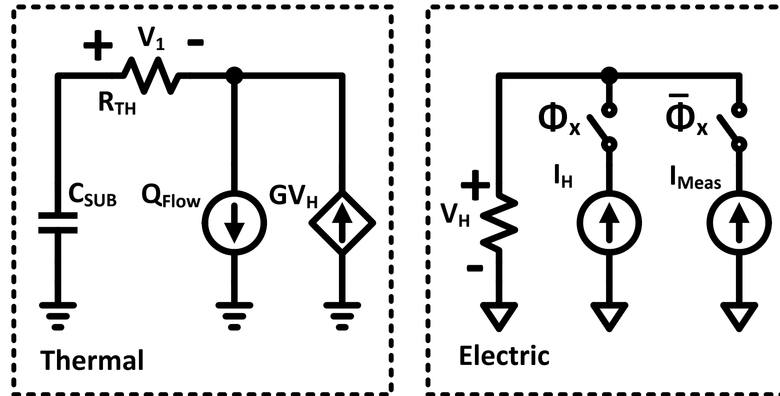

Figure 3.1: Thermal-electrical model of single-element flow sensor. A resistive element is actively heated and passively cooled, and its change in resistance is used to measure flow rate over the element.

3.2 Dual-Slope Control Methods

The fundamental action of the single-element flow sensor system is modeled as charging and discharging a capacitor. As such, looking to the world of analog-to-digital converters (ADC), a dual-slope ADC operates using a similar fundamental principle and can be used to develop a control and measurement architecture.

3.2.1 Dual-Slope ADC

The dual-slope ADC is a conventional ADC often used in bio-sensing and photodiode applications where the primary signal is a small changing current [7, 16]. The dual-slope ADC works in two phases an integration phase and a de-integration phase. During the integration the signal current of interest is stored into an integration capacitor for a fixed amount of time. Then the signal is de-integrated at a fixed rate for a variable amount of time. This second phase is measured and counted. The resulting count value for the variable second slope is the reported measurement for the signal.

3.2.2 Dual-Slope Flow Measurement

The single-element flow sensor can work in the same manner as a dual-slope ADC by taking advantage of the thermal properties of the system. Instead of charge being stored into a capacitor, the system will store heat using its own thermal capacitance. As the system stores more heat, the temperature of the heating element will rise. This rising temperature changes the resistance of the element. The flowing fluid will take away the heat, effectively discharging this thermal capacitance. While discharging, the temperature of the heating element will fall. As with the dual-slope ADC, the dual-slope flow measurement has two separate phases: a fixed-time heating phase, and a variable-time discharge or measurement phase, as illustrated in Fig. 3.2.

In the heating phase, the sensor element acts as a resistive heater, converting electrical energy into heat. In order to ensure that the same amount of energy is placed into the system each heating phase, the power supplied to the heating resistor is kept constant, even as the resistance changes. For each heating phase, the energy added into the system using this constant power approach is:

$$E = P_{heat} * t_{heat} \tag{3.1}$$

At the end of the heating phase, the system is switched into the measurement phase. During the measurement phase, a small fixed current is supplied to the element. As the element cools, its resistance changes. The fixed current into the changing resistor creates a changing voltage, which is proportional to the temperature change of the element. This measured voltage is compared with a reference voltage, and a counter counts the time it takes the to cool the element until it passes below the reference, where the system returns to the heating phase for the next measurement (Fig. 3.2). The measurement is reported as the number of counts counted in the measurement phase. As the flow rate increases, the system will cool faster, discharge the heat more quickly, and the measured count value will decrease. As the flow rate decreases, the system will take longer to cool, increasing the measured counts per phase.

The dual-slope thermal flow sensor scheme has an additional consideration when compared with the dual-slope ADC it is modeled after. Any thermal flow sensor is inherently non-linear, as heating and cooling are exponential processes. Due to this, the dual-slope measurement method is also nonlinear. In addition, the fluid flow is constantly

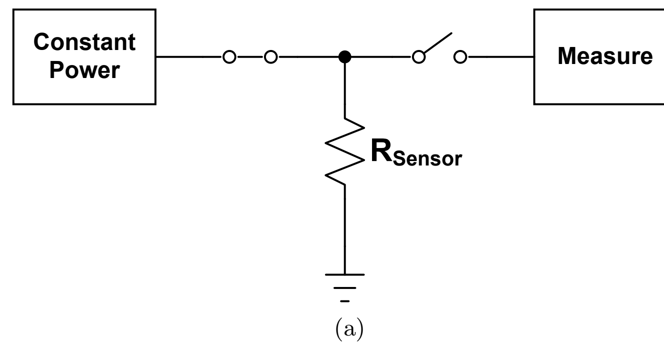

(a)

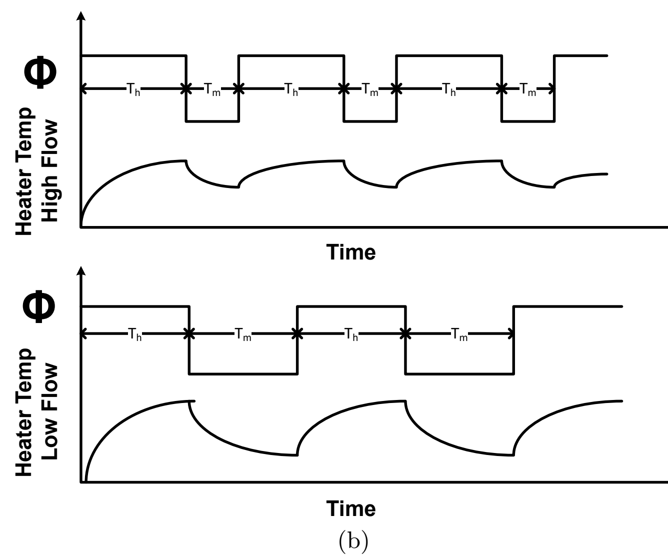

(b)

Figure 3.2: Dual-slope timing diagram

pulling heat out of the sensor element, regardless of phase (Fig. 3.2). As the element is heating, heat is also removed from the system, and the temperature at the end of the heating phase is itself a function of the fluid flow rate. This reduces the total resistance change available for the system to measure, reducing the precision of the measurement. This dual nonlinearity, in both heating and cooling, will lead to a reduced measurement range and degraded precision at high flow rates.

3.3 Discrete Single-Element Flow Sensor System Design

An experimental test setup was implemented using discrete circuit elements on a printed circuit board (PCB) to test the dual-slope single element flow sensor. A block diagram of the dual-slope control and measurement circuits is shown in Fig. 3.3. It includes the needed test circuitry: a constant power regulator, a resistance measurement circuit consisting of a configurable current source, summing amplifier, comparator, and access to an Opal Kelly FPGA module. The needed circuitry were implemented discretely on a test PCB. A photo of the complete test PCB is shown in Fig. 3.4. Additional details of each of the system components are provided in this section.

3.3.1 Constant-Power Regulator Circuit

The element is expected to undergo a significant change in resistance during the heating cycle. If the element is to be heated using a constant current source the power would increase linearly with the resistance. With a constant voltage source, the current will fall exponentially with resistance. These changes in power will introduce distortion into the flow measurement signal and reduce the dynamic range of the flow sensor. To mitigate these concerns, a constant power regulator is used for the heating circuit. The constant-power sub-circuit utilizes a current measurement integrated circuit (MAX4211E), which includes a current sense amplifier and an analog multiplier. A schematic of the circuit is shown in Fig. 3.5. This is used to produce a signal that is proportional to the power supplied to a monitored branch. Using this signal in feedback with an op-amp and p-channel MOSFET, a linear regulator is formed, where the load voltage is changed to maintain a constant power across the load. Constraints for the design of the feedback network include: the analog multiplier full-scale voltage at the load voltage input is ap-

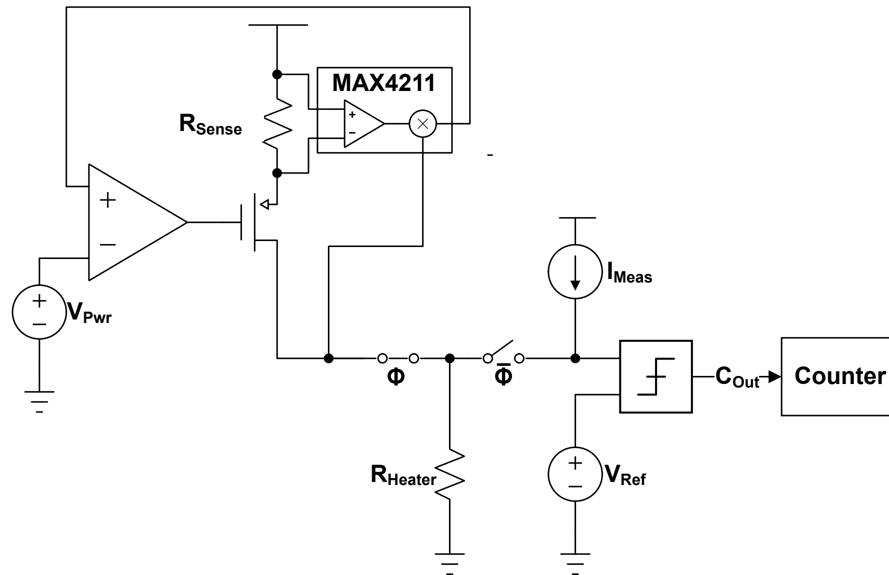

Figure 3.3: A block diagram of the top level of the discrete single-element flow sensor PCB.

Figure 3.4: Photograph of the completed test PCB used to test the dual-slope control algorithm using the single-element thermal flow sensor.

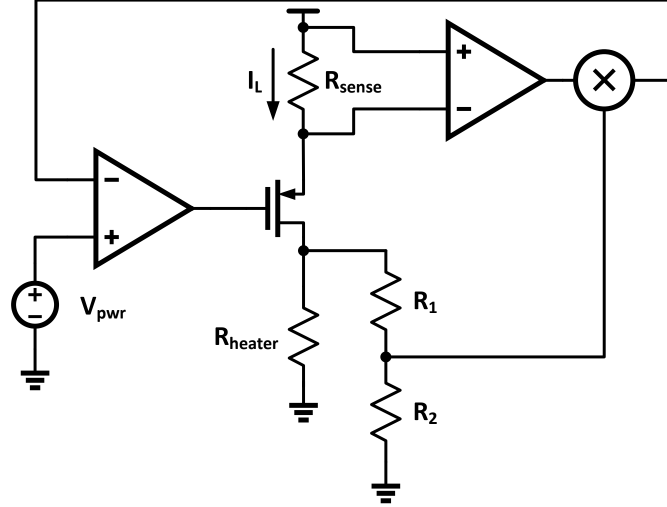

Figure 3.5: A schematic of the constant power regulation circuit

proximately 1 V, and the full-scale sense voltage of the current sense amplifier is 250 mV. Designing to cover the worst case R_1 and R_2 were picked to ensure that:

$$1\,V > \frac{R_2}{R_1 + R_2} * 5\,V \tag{3.2}$$

In addition, R_2 and R_1 were picked as high-value resistances to minimize power loss through the measurement circuit. The sense resistor is chosen to allow the maximum amount of current into the load resistor:

$$150\,mV > I_{lmax} * R_{sense} \tag{3.3}$$

When all parts are combined, the output voltage is proportional to the power supplied by the constant-power regulator:

$$V_{pwr} = 25 * I_l * R_{sense} * \frac{R_2}{R_1 + R_2} * I_l * R_l \tag{3.4}$$

$$V_{pwr} = 25 * R_{sense} * \frac{R_2}{R_1 + R_2} * P \tag{3.5}$$

3.3.2 Resistance Measurement Circuit

The resistance measurement circuit is designed to measure the change in resistance of the sensor element as it cools. It does this by injecting a small test current into the element, and the voltage across the element is fed to a comparator with a reference. The comparator output is then sent to an FPGA, which runs the dual-slope measurement control algorithm. The current is generated by an adjustable current source IC (NXP PSSI2021SAY), where the current output is controlled using an external resistor and is set equal to:

$$I_{out} = \frac{0.617}{R} + 15\mu A \tag{3.6}$$

The external resistor, R, is implemented using a digital potentiometer to provide control of the current source output value using the FPGA. This current is supplied the heating element, and the voltage across the heating element is input to a non-inverting summing op-amp circuit to provide a DC level shift and optional signal amplification. The DC level shift is needed to shift the sensor element voltage signal to within the comparator's input operating range. A comparator is included in the current measurement IC (MAX4211E). This is used in conjunction with a built-in band-gap reference voltage generator, which is adjusted using a potentiometer to provide the comparator reference voltage.

3.3.3 FPGA-Based Dual-Slope Sensor Control

An FPGA is used both for control of the flow sensing circuitry, and to collect and export measurement data for downstream processing. An integrated FPGA module is used (Opal Kelly XEM3610-LX45), which includes on-board memory and a high-speed USB3.0 data interface. Data collection is accomplished using the Opal Kelly Front Panel interface and application programming interface (API). A high-level architecture for the FPGA operation is shown in Fig. 3.6, which was implemented in verilog.

The Opal Kelly interface is a collection of pre-built modules that allow for an API to connect the FPGA and MATLAB. The data out from the comp block shown in Fig.3.6 represents the measured flow value from the dual-slope controller described below. The remaining logic in the FPGA is glue logic connecting the dual-slope controller to the Opal Kelly interface, an I2C master module that is used to talk to the digipot described in

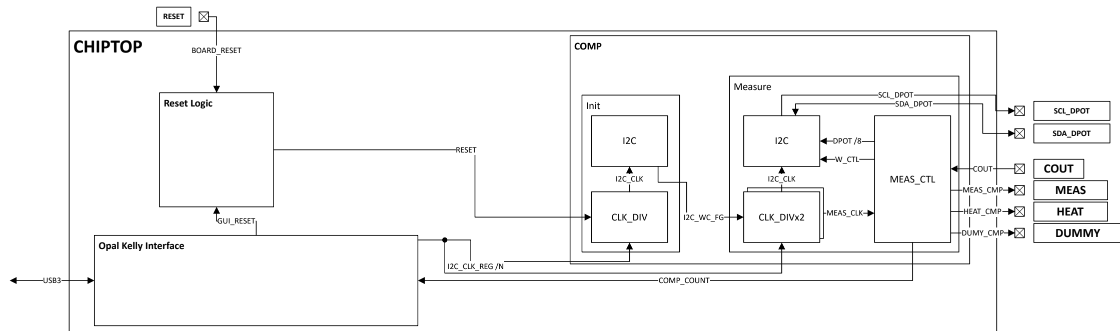

Figure 3.6: Block diagram of the FPGA

3.3.2, manual control over all needed switches for debugging, and a global reset generator.

The dual-slope controller state machine consists of six states, which provide control for the constant-power regulator, resistance measurement circuits, and all other external logic blocks to implement the dual-slop measurement algorithm (Sec. 3.2.2):

Idle State machine default. When an enable signal is generated from the MATLAB graphical user interface (GUI), the system moves into the heating on state.

Heating Current On The constant-power regulator is turned on to supply a heating current and starts the heating timer. After the programmed heating time has elapsed, the state changes to the heating off state.

Heating Current Off The heating current is switched off, followed by a delay of 4 clock cycles, before moving to the measure on state. The delay is in place to generate non-overlapping phases between the measurement circuitry and heating circuitry to prevent the heating circuitry from damaging the measurement circuitry.

Measurement Current On The measurement current is supplied to the element, and the state moves into the measurement state.

Measurement The comparator is first unlatched, making it transparent. After a delay, the comparator is latched, and the output is read. If the comparator output is high, this indicates that the heater is still hotter than the reference temperature; a counter is incremented, and the cooling/measurement process repeats. If the comparator output is low, the heater has cooled below the reference temperature. The

total count of cooling/measurement repeats is updated for export to the MATLAB interface, and the state moves to the measurement off state.

Measurement Current Off The measurement current is switched off, and after a delay the state returns to heating.

In all states if the enable signal goes low, the system moves to the idle state.

3.4 Resistive Sensor Element

For the single element shown in Fig. 3.2a, a thermorestive style element is used due to its ease of manufacturing for a discrete component to test the dual-slope algorithm and also as precursor to further integration of the element on a IC scale. The resistive sensor element is made out of metal on an epoxy disk. The section below will further describe the physical and electrical design of the elements.

3.4.1 Sensor Element Design Considerations

For a conductive material, resistance, R, changes with temperature according to its temperature coefficient of resistance, α, as

$$R = R_{nom} * (1 + \alpha \Delta T) \tag{3.7}$$

where R_{nom} is the nominal element resistance and ΔT is the relative change in element temperature. Used as a single-element flow sensor, the resistive element will be heated due to Joule heating, where current flow through a resistive element dissipates power proportional to the resistance and square of the current. The resulting temperature change in the element due to the power dissipated, P, depends on the heat capacity, c, of the element material and is described by

$$\Delta T = \frac{Pt}{cm} \tag{3.8}$$

for time, t, and mass, m.

Electrically, (3.7) suggests that the greatest change of resistance will come from a large resistor with a high temperature change, and the temperature change is maximized

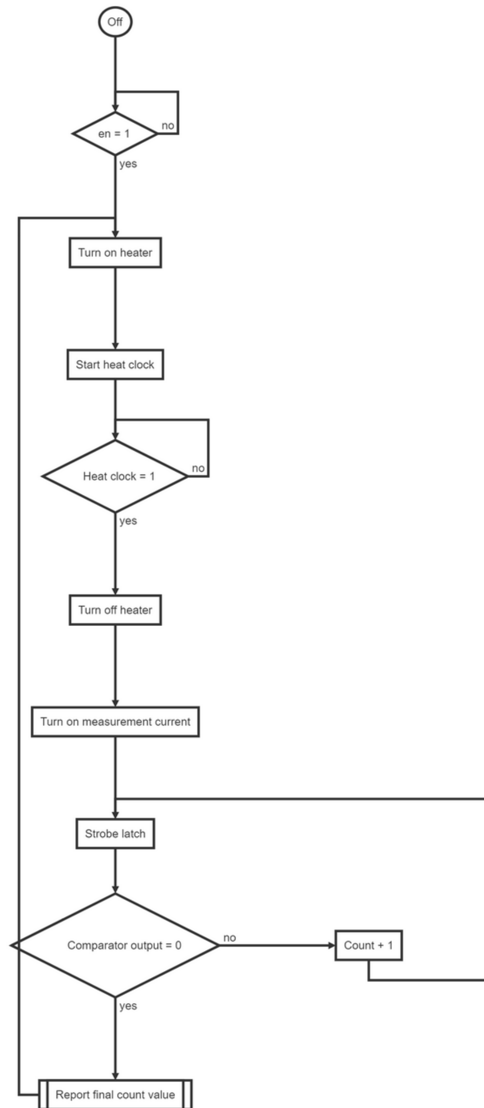

Figure 3.7: Diagram of the dual slope measurement state machine.

by dissipating the largest amount of power possible in an element with low mass, as described by (3.8). However, in a system with a fixed supply voltage, these two goals force an inherent trade-off in element design. The element's resistance value needs to be selected low enough such that sufficient power can be dissipated to achieve appreciable temperature change, and the resistance value needs to be selected high enough to cause measureable flow-induced resistance change. For this design, with a maximum voltage of 5 V a nominal resistance of 500 Ω balances these trade-offs.

The sensor element material is selected to maximize the temperature change per energy applied, which is a function of temperature coefficient of resistance, density, sheet resistance, and heat capacity. To maximize temperature increase and resistance change, the element material must exhibit low mass, low specific heat, and a high temperature coefficient of resistance. Two CMOS-compatible materials fit these specifications well, aluminum and tungsten. For this design, aluminum was chosen for ease of sensor element fabrication.

3.4.2 Sensor Element Design and Fabrication

The sensor element is designed assuming thermally evaporated aluminum with a thickness of approximately 500 nm. The metal is defined as a serpentine pattern with 25 μm wide traces and a trace spacing of 25 μm. To achieve the targeted resistance of 500 Ω, a total trace length of approximately 23 cm is required, resulting in 230 turns for a 1 mm wide element. The layout for the element was implemented in Cadence Virtuoso, and the CAD layout of the element on its epoxy disk is shown in Fig. 3.8a. The layout was used to fabricate a chrome-on-glass photolithography mask.

A thin (∼1 mm) sheet of semiconductor-grade epoxy is used as the build substrate to provide thermal isolation. The epoxy wafer is cleaned using an O_2 plasma, followed by a spun layer of SU-8 2005 for substrate planarization. After soft baking, a flood exposure and hard bake permanently cure the SU-8 layer. A lift-off mask is patterned using a two-step photoresist process; lift-off resist (LOR, Microchem) follow by a standard positive photoresist (SH1818, Microchem) and exposed through a chrome-on-glass photomask. After development, a final O_2 plasma clean removes any remaining residue. A thin chrome adhesion layer is applied, followed by approximately 500 nm of evaporated aluminum. The excess metal is removed from the wafer via a lift-off process using

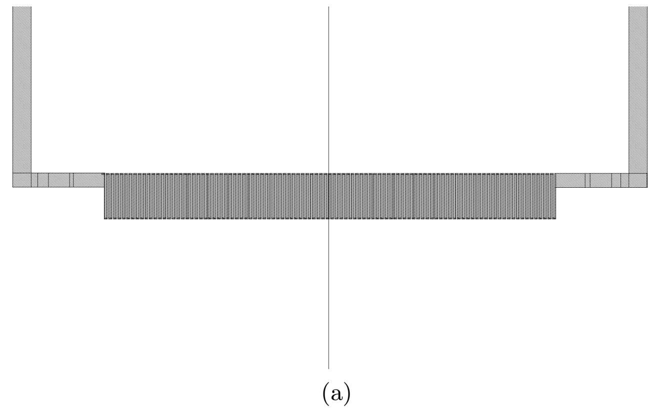

(a)

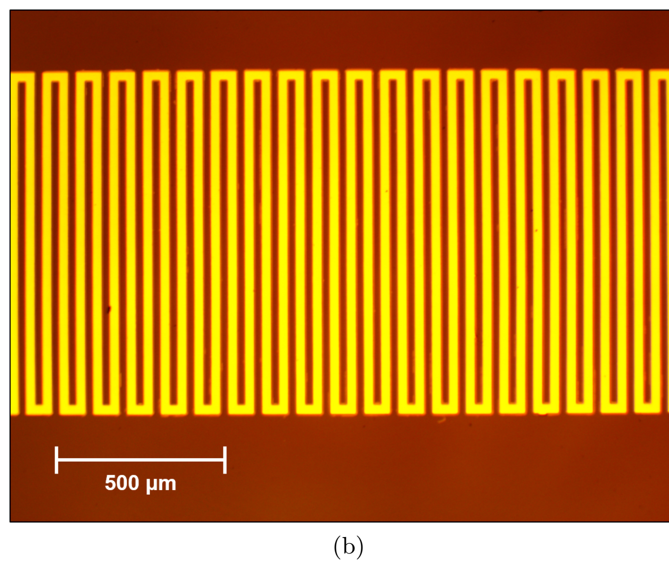

(b)

Figure 3.8: (a) Layout of the element in Cadence Virtuoso. (b) Microscope image of a section of the manufactured element

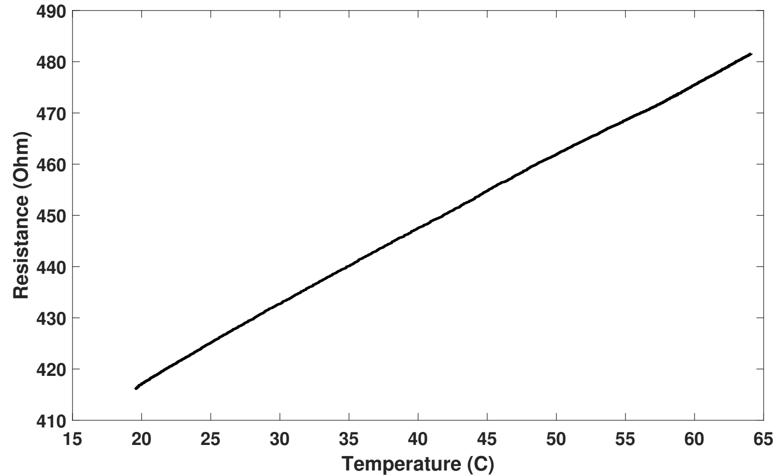

Figure 3.9: Manufactured element's resistance across temperature

Remover PG (Microchem). A section of the element is shown in Fig. 3.8b.

After fabrication, the epoxy wafer was cut down to fit inside the test environment, and wires were attached to the pads using silver epoxy. The manufactured element measured 461 Ω at 19 C.

3.4.3 Sensor Element Thermal Characterization

The element's resistance was characterized over a wide temperature range. This was done by placing the element into a gravity convection oven and heating the element while measuring the temperature and resistance of the element. The element resistance was first measured a 19 C and then placed in the oven to bake to 64 C. During this baking process, the temperature of the element was monitored and logged using a Reed SD-967 Thermometer with a K-type thermocouple placed on the epoxy substrate. The sampling interval for the temperature measurement was 1s. The resistance was measured and logged using a Keithly 2100 multimeter sampling every 1 s.

The change in sensor element resistance over the tested temperature range is shown in Fig. 3.9. The element has a nominal resistance of 416.2 Ω at 20 °C. A total change in resistance of 65.4 Ω was measured with 44.6 °C of temperature change, ΔT. This represents a temperature sensitivity of $1.464\,\Omega/^{\circ}C$ and a measured temperature coeffi-

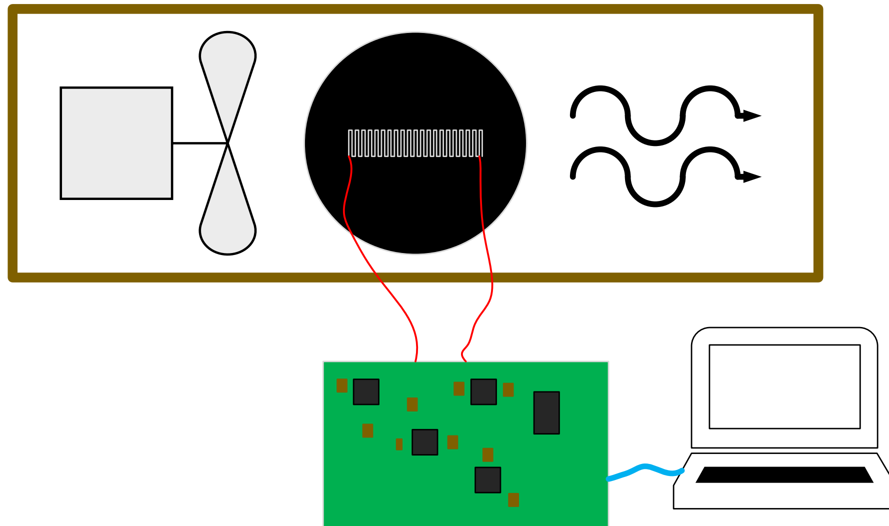

Figure 3.10: Fan-based flow sensor test setup

cient of resistance of $0.0035\,C^{-1}$, which is less than the common bulk material value of $0.00429\,C^{-1}$.

3.5 Discrete Dual-Slope Flow Sensor Testing

3.5.1 Experimental Setup

Initial tests of the flow sensor were done using a fan-based system to produce a variable rate of airflow across the element. A high-level illustration of the measurement setup is shown in Fig. 3.10. A 2" brushless DC fan was operated using a control voltage from approximately 0-300 RPM. The sensor element was placed downstream from the fan, and both were placed inside an enclosure to direct airflow across the sensor element surface. The control PCB (Sec. 3.3) and laptop were placed outside the enclosure.

3.5.2 Variable Flow Rate Measurement Results

During the heating phase, the sensor element was heated with a constant power of 115 mW. The heating time, T_h (Fig. 3.2b), was set to 1 s, and air flow varied sequentially from no flow through four different fan speeds: 0 RPM, 117 RPM, 196 RPM, and

270 RPM. The measured cooling time, T_m (Fig. 3.2b), is plotted over the course of multiple fan speed settings in Fig. 3.11a.

A histogram of the data, shown in Fig. 3.11b, shows the T_m grouping from each flow level tested. Each level has a distinct peak with little overlap between the fan levels, indicating sufficient resolution at these flow rates. For this setup, an independent flow meter was not used, and absolute flow rate could not be quantified.

3.5.3 Variable Heating Time Measurement Results

Using the dual-slop control algorithm (Sec. 3.2.2), the heating time, T_h, was varied to characterize sensor and system responses. The heating time was tested at 100 ms, 1 s, 5 s, and 10 s. The results are shown in Table 3.1. Looking at the results, an increase of heating time generally increases the signal-to-noise ratio, but has increased drift and decreased linearity are observed at higher flow rates.

Table 3.1: Different cooling times due to variation of the sensor's heating time

Heating Time	**Cooling Times For Varying Fan Speeds (s)**			
	0 RPM	***117 RPM***	***196 RPM***	***270 RPM***
100 ms	0.164	0.12	0.094	0.084
1 s	1.111	0.818	0.603	0.403
5 s	4.506	2.617	1.666	1.315
10 s	7.287	4.139	2.503	1.506

3.6 Metered Flow Sensor Tests

The fan-based testing possesses several limitations in its ability to accurately determine the sensors ability to respond to flow. The control over the fan's speed is coarse and despite the fan's speed being proportional to its flow rate, determining the actual flow rate from the fan is unfeasible. In addition, the air-flow the fan provides is non-laminar. A new metered flow chamber was designed and built to alleviate these concerns, and additional testing was performed with the chamber. This section describes the design of a metered flow chamber and the tests and results obtained from it.

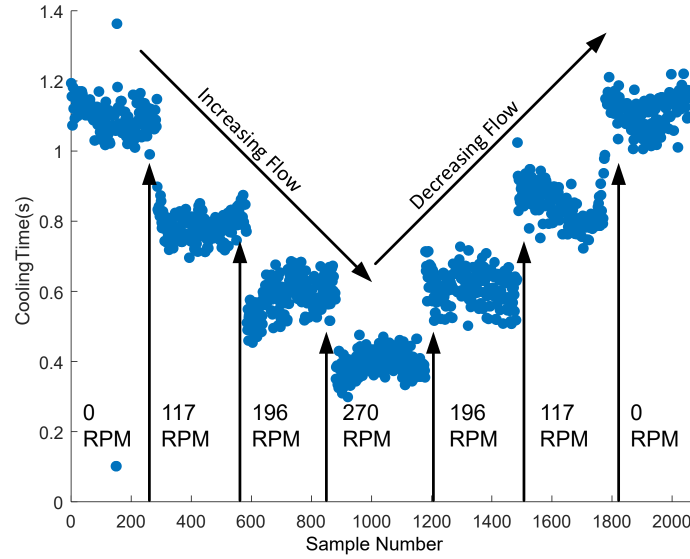

(a)

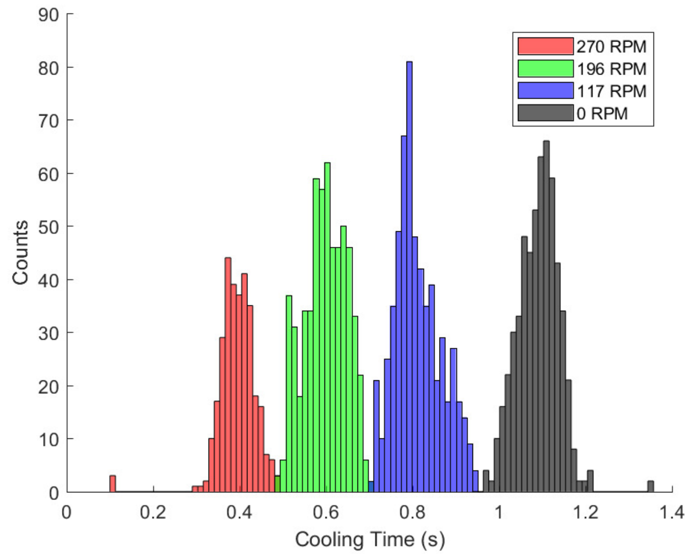

(b)

Figure 3.11: (a) Measured cooling time (T_m) for the single-element sensor under varying air flow. Arrows indicate sample at which fan speed was changed. (b) Histogram showing the distribution of cooling time (T_m) at each tested fan speed, as an indication of measurement noise and resolution.

3.6.1 Experimental Test Setup

Flow Chamber

To improve test precision, a metered flow chamber was constructed. The metered flow chamber uses a compressed air source feeding a precision flow regulator. An inline electronic flow meter (King Instruments) provides a measurable flow range of 0.8-8.2 SCFM with an accuracy of ±3%. The flow regulator is shown in Fig. 3.12.

The air leaves the flow regulator through 1/4" flexible tubing and feeds 2" PVC pipe end cap; a length of 2" PVC pipe serves as the flow chamber. Due to the difference in the diameter of the tubing and the pipe, the flow is not laminar. To smooth out the air-flow, a two-part, 3D-printed baffle was designed (Fig. 3.13) and installed into the tube. The airflow with the baffle is laminar near the final baffle output.

Test Element Installation

The sensor element was installed through a hole cut into the top of the pipe, as shown in Fig. 3.14, and placed approximately 3" downstream of the final baffle component to promote uniform flow across the element. The element was secured to the middle of the flow chamber. K-type thermocouples were installed on the test substrate, in the flow chamber away from the test element, and outside the flow chamber on the test PCB. During all tests, several temperatures were measured using the Reed SD-947 thermocouple reader.

3.6.2 Variable Flow Rate Measurement Results

For the initial metered flow sensor tests, the cooling time, T_m, was set to 1 s, and the power set to the maximum allowed, approximately 115 mW. Cooling time, T_m, was recorded by the FPGA in MATLAB with a sampling period of 1 s. The sensor started at room temperature and was allowed to warm up for 30 minutes of continuous cycling with no forced airflow. After the warm-up period, the flow rate was initially set to 0.8 SCFM. The flow rate was held at this rate for 5 minutes and then adjusted in steps from 0.8 SCFM to 2.0 SCFM, with a hold time of 5 min at each rate setting.

Figure 3.15 shows the recorded cooling time of the dual-slope flow sensor in the

Figure 3.12: Flow adjustment valve and meter

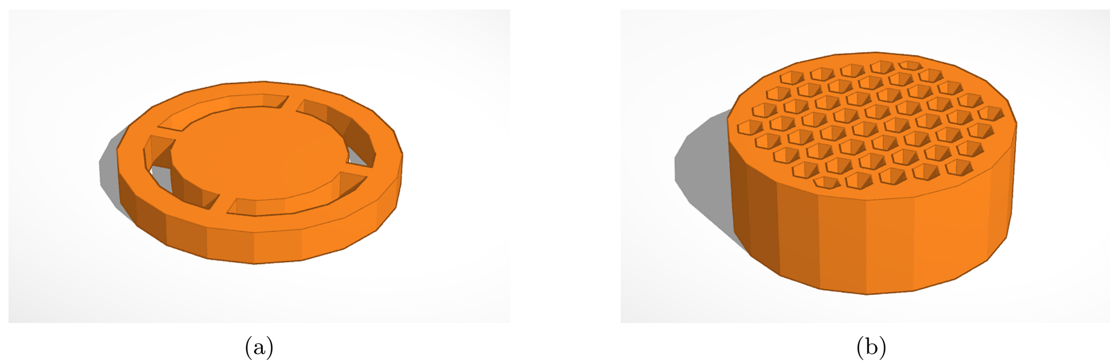

(a) (b)

Figure 3.13: Model of the two-part baffle used to smooth out the air flow in the flow chamber.

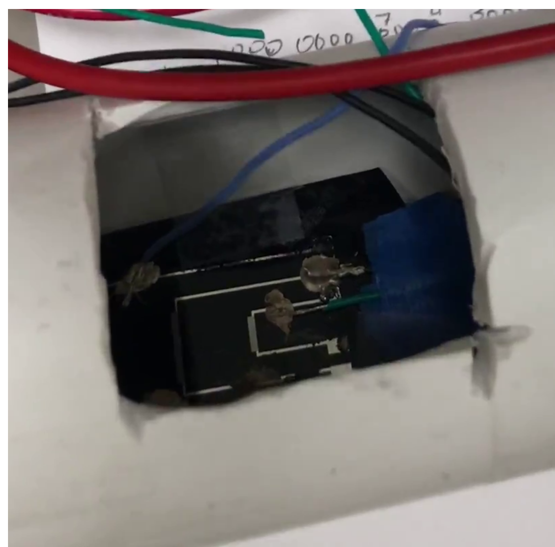

Figure 3.14: Picture of the element installed into the metered flow chamber

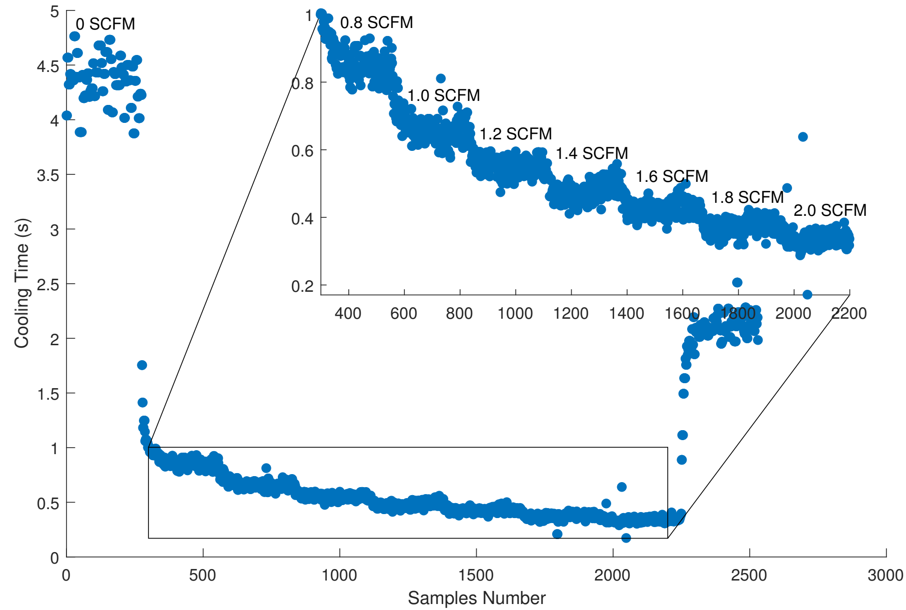

Figure 3.15: Dual-slope flow meter demonstration with 1 S heating time.

metered flow chamber. The inset shows the devices response to the flow steps and shows defined levels for cooling time for each step. One trend to note is the difference in starting and ending cooling values for 0 flow. This difference is believed to be due to the epoxy substrate slowly storing heat as the test persisted.

Figure. 3.16a shows the sensor element warm-up period with no flow from the sensor, starting at room temperature. As the substrate and sensor element heat, the cooling time, T_m, first overshoots and then settles to a steady-state value after approximately 15 minutes. During the warm-up period, sensor elements transfer heat into the epoxy substrate, as well as to the element and surrounding air. As more heat is added to the system, it eventually reaches a stable substrate temperature. Decreasing the heating time, T_h, removes the overshoot from the warm-up period, as shown for the $T_h = 100\,\text{mS}$ result shown in Fig 3.16b.

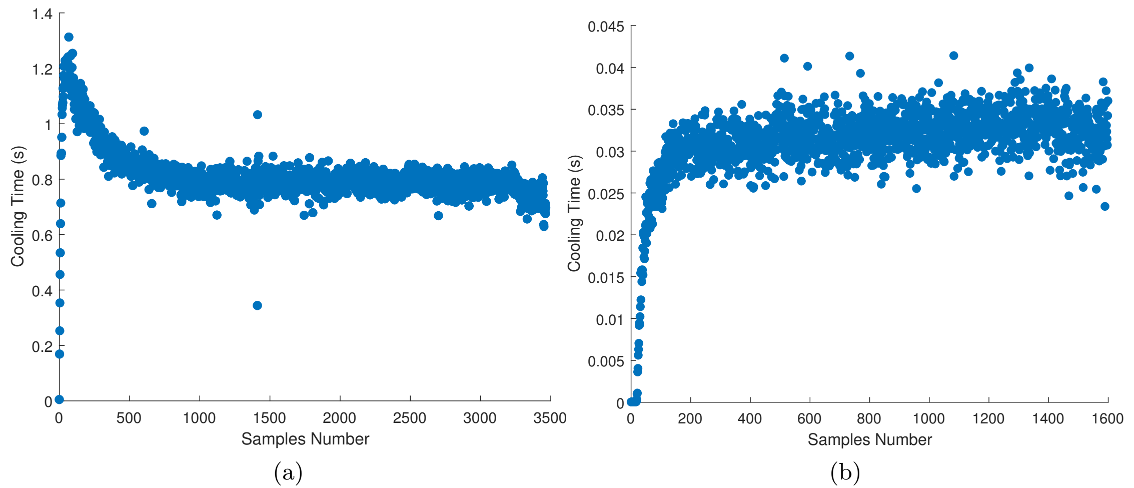

Figure 3.16: Warm-up periods for the element at (a) 1 s heating time (b) 100 ms heating time. Flow levels are annotated over their respective regions.

3.6.3 Variable Heating Time Measurement Results

The dual-slope sensor was also characterized at different heating times, T_h. When the heating time is decreased to 100 ms, as shown in Fig. 3.17a, the sensor is unable to accurately track the flow level, and dynamic range is lost at higher flow levels. When the heating time is increased to 200 ms, as shown in Fig. 3.18a, the dynamic range and accuracy are restored to similar levels as the T_h =1 s flow sensor measurements shown in Fig. 3.15.

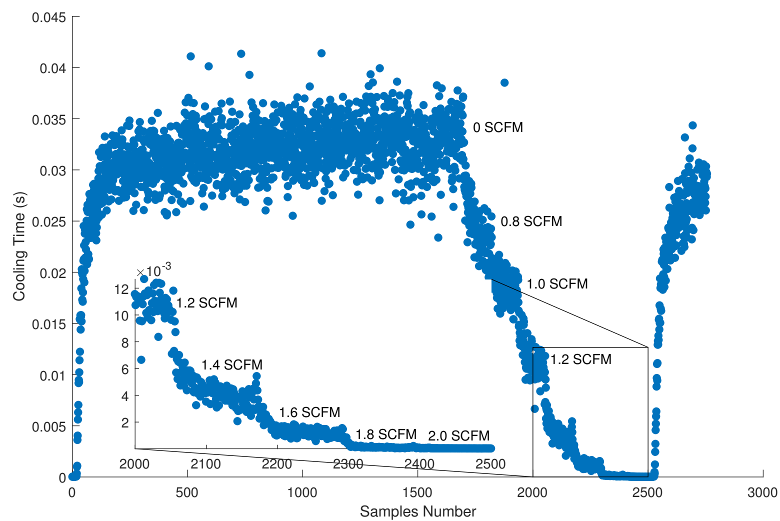

(a)

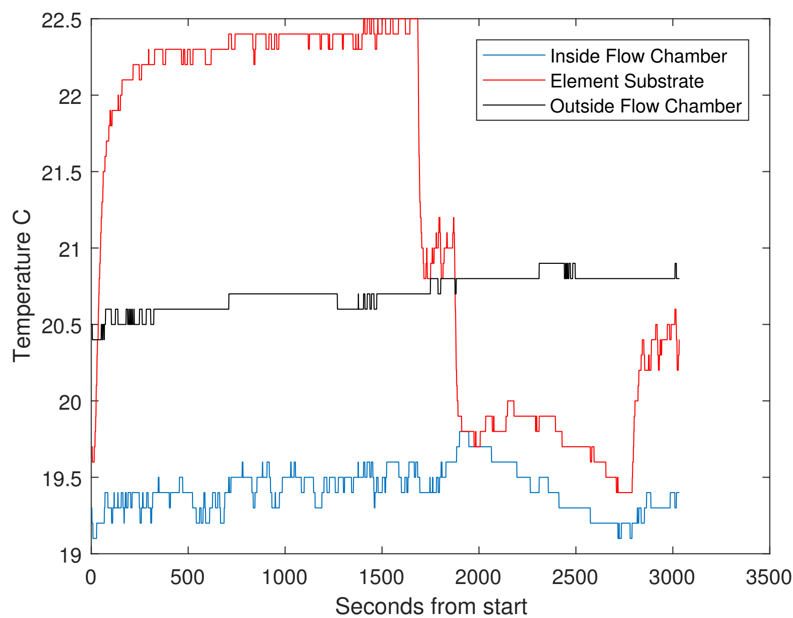

(b)

Figure 3.17: Flow measurement from on-chip element (a) 100 mS heating time, and (b), surface temperature at each system location. Flow levels are annotated over their respective regions.

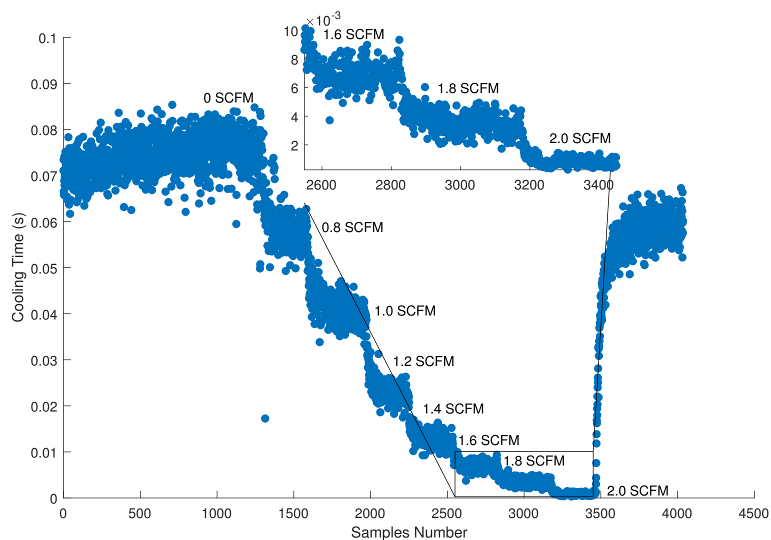

(a)

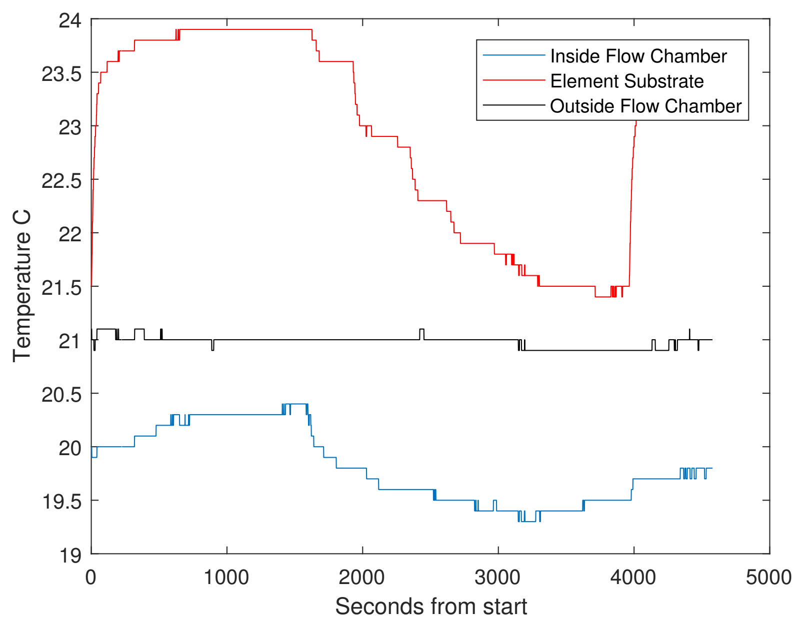

(b)

Figure 3.18: Flow measurement from on-chip element (a) 200 mS heating time, and (b), surface temperature at each system location. Flow levels are annotated over their respective regions.

Chapter 4: CMOS Single-Element $\Delta\Sigma$ Thermal Flow Sensor

The next goal was to integrate a thermal flow sensor into a CMOS IC. Integration of this sensor into a CMOS IC requires exposure to the flow for the potential heating and sensing element. This requires the sensor to be made in the top metal layers. Using metal to make a sensor of large enough value to be sensitive to the flow requires a large amount of area. Including two different elements, a heating element and a sensing element, would further increase the area concerns. In addition to this working in a modern CMOS process means designing with limitations to the maximum allowable voltage for the devices, thus limiting the maximum amount of power allowable for heating. To alleviate these concerns and allow for full CMOS integration, the single element architecture discussed in Chapter 3 was adapted for use in the flow sensor.

4.1 Single-Element Thermal $\Delta\Sigma$ Flow Sensor

Using the single-element thermal flow sensor in the CMOS environment required a few changes to the dual-slope control algorithm presented in Chapter 3. To increase the speed of measurement and better capture temperature change a thermal delta-sigma style modulator was modified for use with a single-element system as shown in Fig. 4.1 [3]. To operate the system with a single element, the element must be split in the time domain to support measurement and heating in two different phases, as shown in Fig. 4.2.

The first phase is the heating phase, where heat is applied for a fixed amount of time. At the end of the heating period, the element is allowed to cool until its resistance reaches a threshold, and then the heater is again turned on for a fixed amount of time. The cooling time is variable, and the control loop seeks to maintain a constant overheat temperature on the heating element. The control loop features a modified $\Delta\Sigma$ modulator to work around the fixed heating phase and the measurement phase. At the end of each heating phase, the measurement phase begins with the starting of the flip-flop's clock. When the element cools, the measurement phase ends and the next heating phase beings.

Each heating phase is summed over an accumulation period to produce a flow mea-

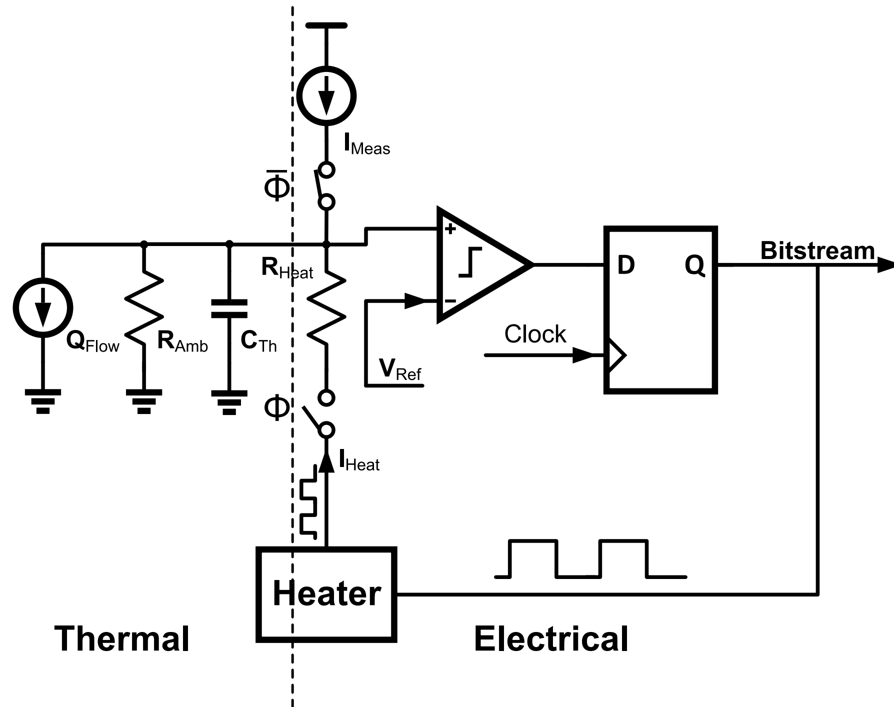

Figure 4.1: Block diagram of the proposed single-element thermal $\Delta\Sigma$ system.

surement. The sum of the pulses represents the amount of heat needed to keep the element above its set overheat temperature. As flow increases, the amount of energy taken away from the system also increases, causing a rise in pulses needed to keep the system above the target temperature. The integration time can be modified in order to produce a faster but less precise flow measurement with a small heating time, or a slower more precise flow measurement with a larger integration time.

4.2 Circuit and Element Design

The single-element $\Delta\Sigma$ thermal flow sensor element and supporting circuitry were designed and fabricated in Tower Jazz 180 nm CMOS process. Two copies of the element and supporting circuity were included, one using an element with the top metal fully exposed to the environment, and another with an SiO_2 passivation layer on top of top metal layer of the element. This section will describe the high-level system design and

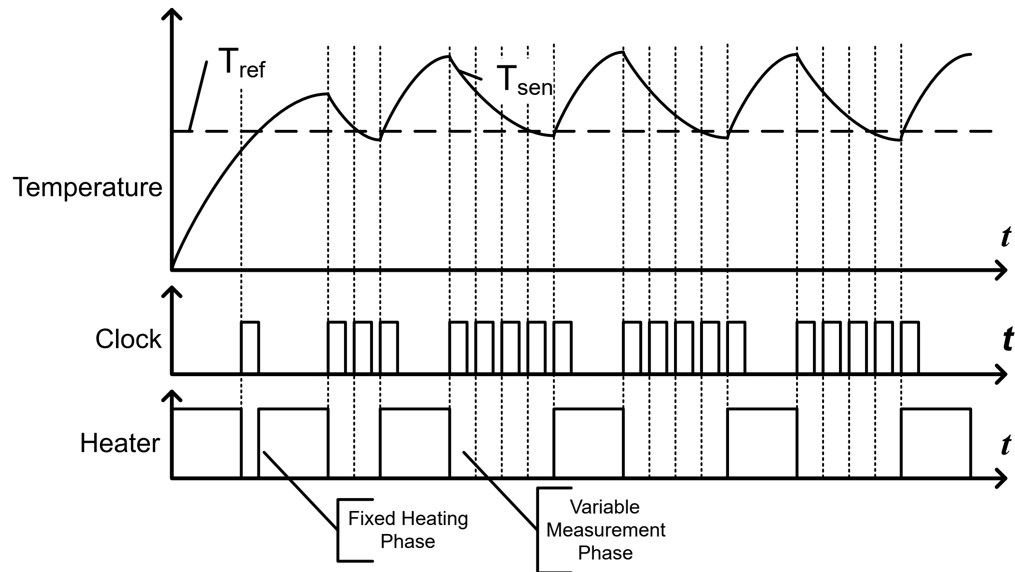

Figure 4.2: Timing diagram of the proposed single-element thermal $\Delta\Sigma$ system.

the design of major circuit blocks.

4.2.1 Top-Level System Design

The system-level goal of the single-element flow sensor circuitry was to facilitate the ability to use an off-chip current source for heating and provide the needed blocks for on-chip element measurement. A block diagram of one copy of the single-element $\Delta\Sigma$ thermal flow sensor IC is shown in Fig. 4.3. On the full chip, two copies exist and the two elements are wired in parallel during the heating phase. In the heating phase, an external heating current source is switched in to heat the elements, and the measurement circuits are disconnected from their respective elements. In the measurement phase, a small constant current is fed into the element. The resulting voltage across the element is then monitored. As the element cools, the resistance will change, and with it the voltage due to the constant current being applied to it. This voltage is boosted by a DC level boosting circuit and fed into a comparator. While measured resistance is higher than the reference applied off-chip, the comparator's output is high and the element continues cooling. Once the element resistance falls below the reference the system ends its measurement phase

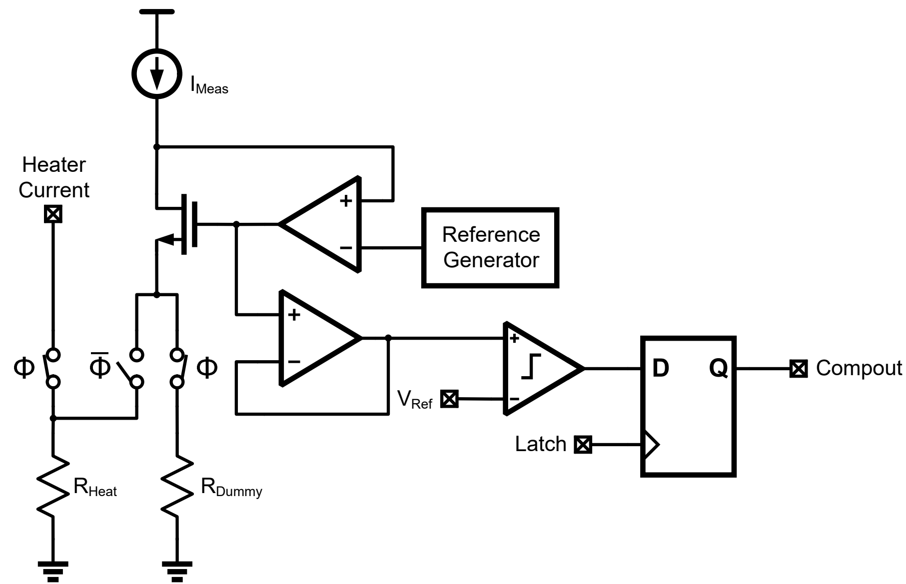

Figure 4.3: Block Diagram of the Flow Sensor Chip.

and the system is switched into heating mode again. During the measurement phase, the heating current is switched off, and each element is switched into their measurement circuits. To enable flexibility in the measurement range, the current source is a 10-level thermometer-encoded current source allowing for measurement current in the range of $15\,\mu$A-$150\,\mu$A. The flip-flop latches the comparator output for the control logic off chip.

4.2.2 Thermometer-Encoded Current Source Design

The current source, schematic is shown in Fig. 4.4a; this is a thermometer encoded current source with 10 individual levels of approximately $15\,\mu$A each. This gives the total measurement current range of $15\,\mu$A-$150\,\mu$A. Each unit current cell is a single P-channel MOSFET with its switching circuitry on the gate rather than the drain node. This was done to avoid switch resistance in the path of the measurement current. When the switch is turned on, the bias voltage is passed through the NMOS to the gate of PMOS current regulation device. When the switch is off, the PMOS switch pulls the gate to the supply voltage, turning that section of the current source off. The layout of the complete current source is shown in Fig. 4.4b.

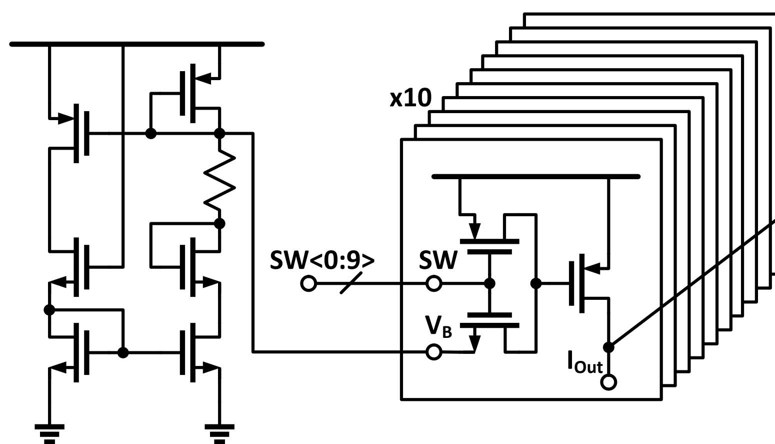

(a)

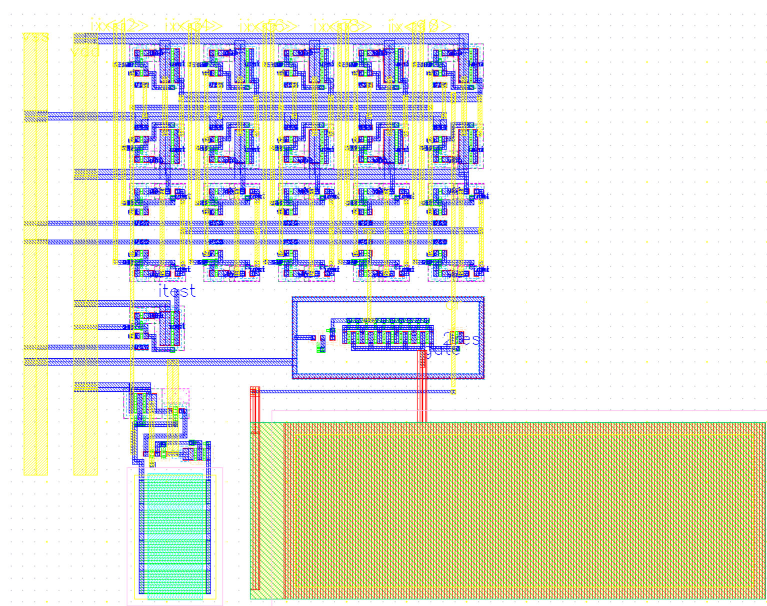

(b)

Figure 4.4: Schematic and layout of the thermometer encoded current source, (a) schematic (b) layout.

4.2.3 DC Level Boosting Circuit

Between the output of the current source and the element is a DC level boosting circuit. This is needed to pull the measurement voltage generated from the element into the operating range of the comparator. The DC level boosting circuit is a pseudo low dropout voltage regulator. It is comprised of a N-channel MOSFET between the current source and the element, and an op-amp to control the gate bias. The op-amp has its inverting terminal connected to the drain, or output node, of the current source, and the non-inverting input is connected to a reference voltage generator, schematic is shown in Fig. 4.6. As the element resistance changes, the MOSFET's source voltage changes. In response to this the op-amp will adjust the voltage on the gate node to keep the drain voltage constant. This adjustment is 1:1 with the changes on the source node giving the measured signal plus a DC level shift. A dummy n-poly resistor of matching value ($500\,\Omega$) is also included and switched into the measurement circuit during the heating phase. This allows level shifter's control loop to stay near the measurement value, increasing stability and response time.

4.2.4 Comparator Design

The comparator is an op-amp based comparator with two inverters on the output. The schematic and layout are shown in Fig 4.7a and Fig. 4.7b respectively. This topology is chosen to provide the lowest offset voltage possible in order to extend the measurement range. The op-amp is a classic NMOS-input two stage op-amp designed using a $\frac{g_m}{i_d}$ methodology. The input pair, M1 and M2, and output device, M6 were sized for strong inversion for high gain. The current biasing devices, M3, M4, M5, and M7, were sized for weak inversion. The stack of transistors, M12-M15, provide the needed bias voltage and M16 and M17 are there to ensure the bias network starts-up properly.

4.2.5 Element Design

The ideal on-chip heating element is a resistor which should have the following properties:

1. It should be be thermally interfaced with the flow regime above the chip.
2. It should have a sufficiently high resistance value in order to maximize the dynamic

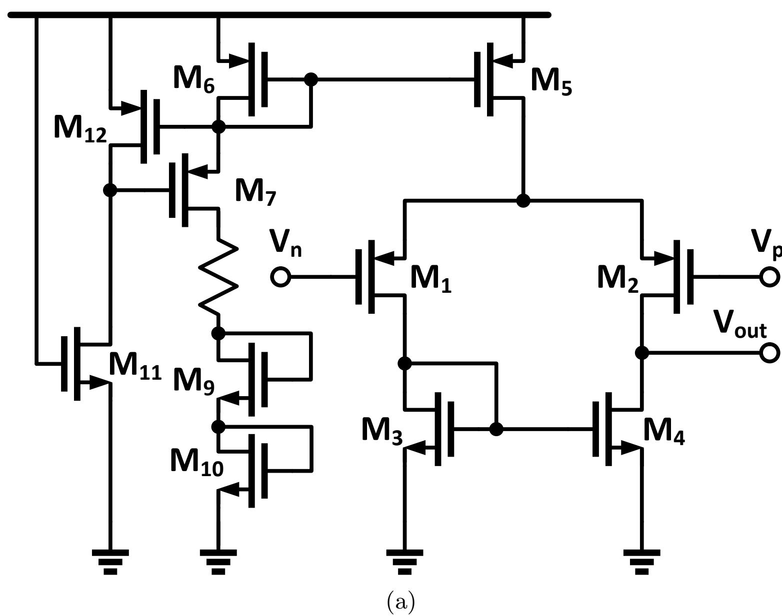

(a)

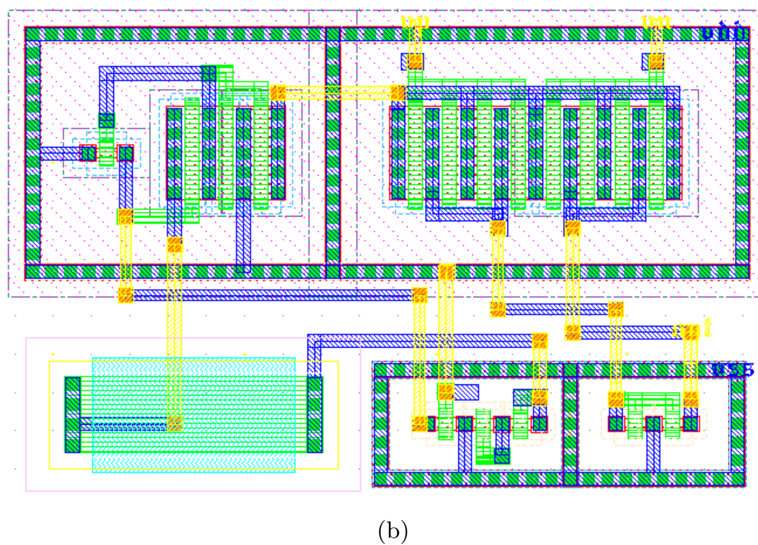

(b)

Figure 4.5: General purpose single stage op-amp used in DC level boosting circuit and as a buffer, (a) schematic (b) layout.

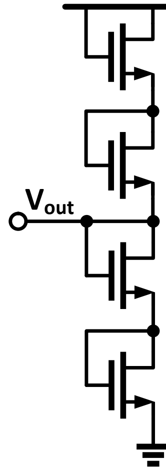

Figure 4.6: Diode ladder reference voltage generator for the DC level boosting circuit.

range of measurable flow rates.

3. The temperature coefficient of resistance, α, should be high, since this defines the lowest measurable change in resistance.

Since the goal was to implement the sensor using standard CMOS structures, the only option that satisfied condition (1) was using the top metal layer to realize the resistor. Indeed, exposed top metal layer structures form the mechanical and electrical contact for I/O pads in CMOS chips. However, in order to satisfy condition (2), the resistor should be at least a few hundred ohms. Designing this using the top metal layer exclusively would have been highly inefficient in terms of area. This is because this layer has extremely low resistivity since its primary purpose is global power routing where minimum interconnect resistance is essential.

One possible option was to use high-resistivity poly-silicon to realize large resistor values with small footprints and interface this with the ambient by using vias all the way to the top metal layer. However, the thermal phenomena would be lost through dissipation into the substrate and the passivation SiO_2. Therefore, the resistive structure needed to be close to the top metal layer.

Tungsten vias have significantly higher resistance compared to the different metal layers. Therefore, a resistor structure that makes use of primarily via resistance can achieve high resistance without occupying nearly as area. The proposed resistor makes

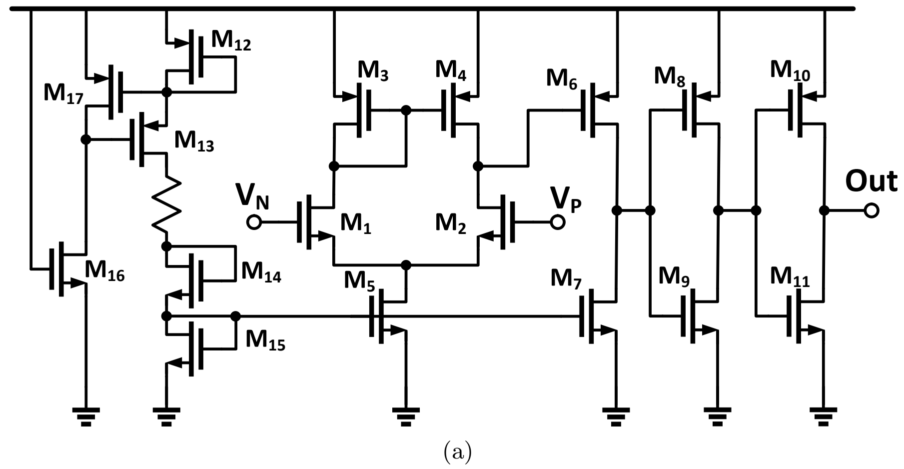

(a)

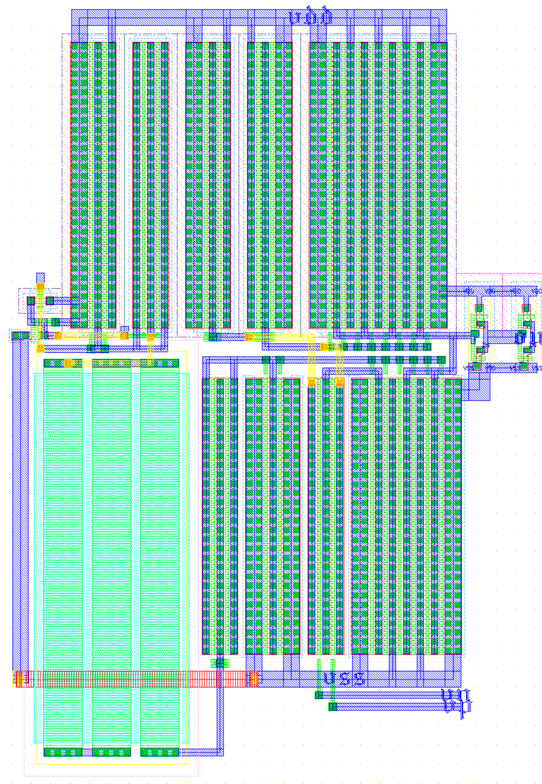

(b)

Figure 4.7: (a) Schematic of the op-amp based comparator. (b) Layout of the comparator.

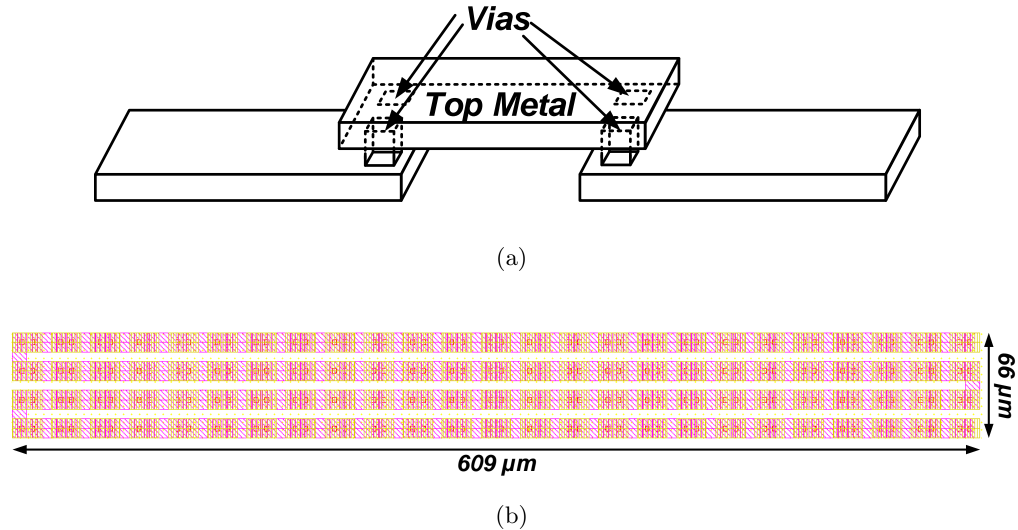

(a)

(b)

Figure 4.8: On-chip resistor where each layer change consists of two vias in parallel. This was done to ensure sufficiently high current densities could be supported, while still maintaining a high resistance density. (a) is a 3-D illustration of the structure and (b) is the layout.

use of a vertically alternating structure between the top metal layer and the next lower metal layer, as shown in Fig. 4.8a. A resistance of $500\,\Omega$ was selected for this design. This satisfied conditions (1) and (2) while also having a reasonable area footprint, as shown in Fig. 4.8b. Almost all of the resistance was contributed by the via resistance and this was validated using extracted simulation results. Unfortunately, because of the restrictions imposed by the design choices, condition (3) was not controllable.

4.2.6 Flow Sensor IC Fabrication

The complete flow sensor, including the resistive sensing element and on-chip measurement circuitry was implemented in a general purpose $0.18\,\mu$m CMOS process. A die photo is shown in Fig4.9. The combined flow sensor and element occupy an area of about $0.39\,mm^2$. After fabrication the chip was packaged in a ceramic open lid package. This style of packaging was chosen to allow the top surface of the IC to interface with the flowing air.

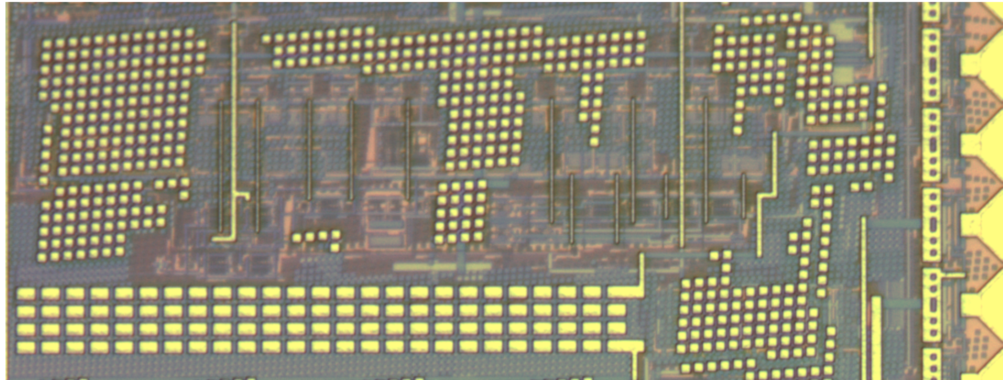

Figure 4.9: Die photo of single element flow sensor

4.3 Test Setup

A printed circuit board (PCB) was made to allow an FPGA module to control the on chip measurement circuitry, switch a current source on and off, and log test data. The FPGA module runs the digital control system for the $\Delta\Sigma$ modulator and reporting the accumulated pulse values to a laptop for data collection. The heating power is provided by an external current source set to give each heater 15 mA of heating current. A regulated flow chamber was made out of a 2" PVC pipe. The pipe has a fitting on one end for regulated compressed air to flow in and a opening on top to allow the flow sensor PCB assembly to slot into the pipe. The compressed air regulation is done with a flow control value into a flow meter. The current measurement setup allows for flow measurements from 0.8 SCFM to 2.4 SCFM. A difference of tubing diameters exists between the regulation and flow chamber and on its own this would cause non-laminar flow in the flow chamber. To smooth out the flow a baffle was designed and placed into the chamber. need to expand and explain each test as well

4.4 Experiments and Results

4.4.1 Element Characterization

The element is characterized for its change in resistance with temperature. To do this the chip is heated while a constant current is fed into the elements and the voltage

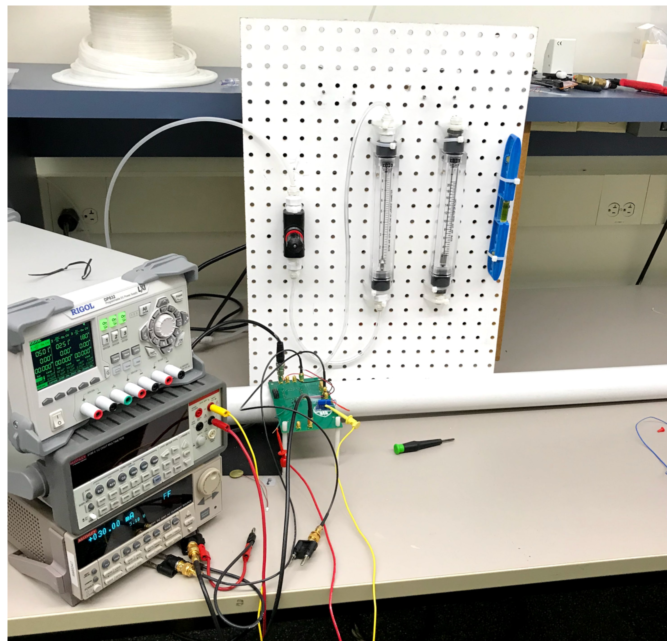

Figure 4.10: The complete setup for the testing of the single-element flow sensor IC installed into the test chamber.

is measured. The two elements are characterized together as one element due to the switching configuration placing them in parallel while heating. The characterization was done using an Agilent current source supplying 10 mA total to the elements, and a Keithly 2100 multimeter was used to monitor the voltage across the input pin to the elements to ground using a . The test PCB was placed into a VWR oven set to heat from 15 °C to about 65 °C. At 65 °C the oven is turned off and the chip allowed to cool in the air. A thermal probe was used to measure the PCB's temperature as the during the heating and cooling process. The Fig. 4.11 shows the changing resistance due to the change in the element's temperature. Over the total 45.2 °C change in temperature the resistance experienced a 20.51 Ω change in resistance. According to this measurement, the element's temperature sensitivity is 0.4538 $\frac{\Omega}{°C}$ and the element's composite experimental temperature coefficient of resistance is 0.0017 $°C^{-1}$. This number is lower than bulk tungsten's value, the material of the vias, the main contributor to the element's resistance, of 0.0045 $°C^{-1}$. The lower value is believed to be be caused by the inclusion of silicon switches. The switches do make up some of the resistance of the element's connection, and they, being silicon, have a negative temperature coefficient of resistance. So as the chip on the whole gets warmer (as in this experiment) their resistance goes down as the elements resistance goes up.

4.4.2 Flow Measurement

Flow measurement is demonstrated by testing the sensor at zero flow and then various flow levels between 0.8 to 1.8 SCFM in the same flow chamber described in section 3.6.1. The sensor is allowed to warm up and then held at each flow level for 10 min before adjusting the air flow to the next flow level. The integration period for each measurement is 3 sec. Each reported measurement point is the average of the integration count values from the 10 min period and the error bars represent ± one standard deviation. The results are shown for different heating times in Fig 4.12a. Two different heating times were tested to see if that would affect the performance of the sensor, 1 mS in Fig. 4.12a and 100 μS in Fig. 4.12b. The results show that the heating time has little effect on the accuracy of the sensor, but the shorter heating interval does allow for more counts in an integration period, increasing measurement fidelity.

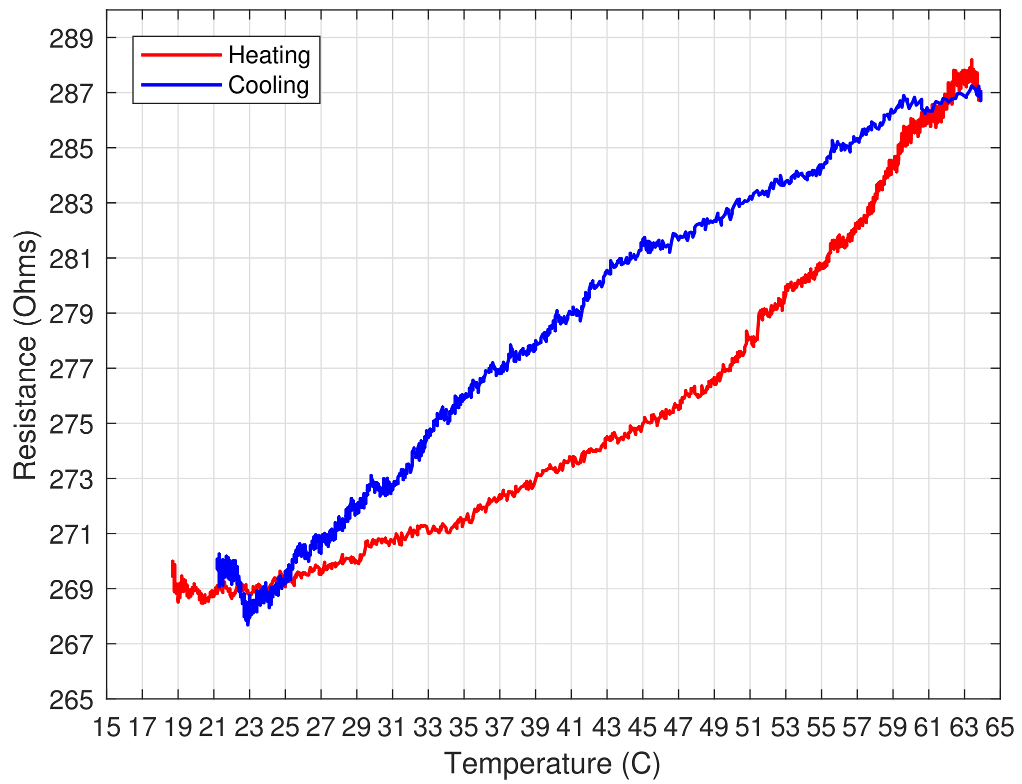

Figure 4.11: Resistance of the two parallel elements as they heat (red) and cool (blue)

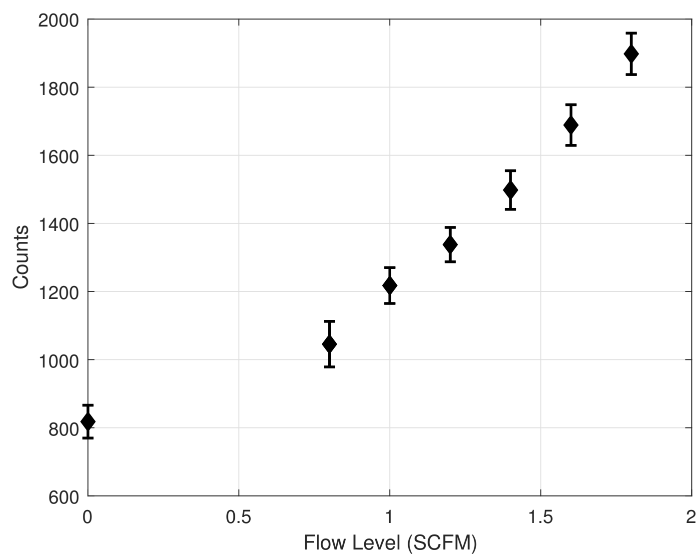

(a)

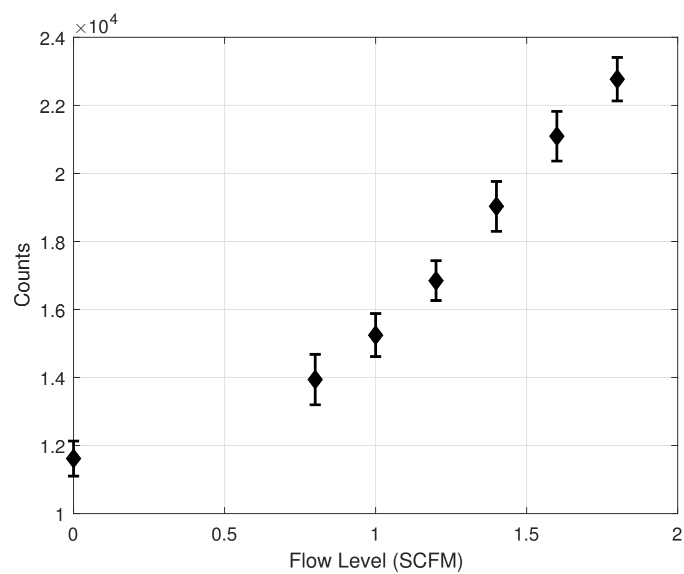

(b)

Figure 4.12: Flow measurement from on-chip element without SiO^2 passivation for (a) 1 mS heating time (b) 100 μS heating time.

4.4.3 Effect of SiO_2 Passivation on Sensor Element

Two different variations of the element were tested: one variation has a SiO_2 passivation layer, Fig. 4.13a, and one without the SiO_2 passivation layer, Fig. 4.13b. Each of these were tested at the 1 mS heating time and under the same flow conditions: the air flow is first off and the sensor is allowed to warm up. Then the air flow level is adjusted from 0.8 to 1.8 SCFM in 0.2 SCFM intervals every 10 min. The results in Fig. 4.13a and Fig. 4.13b show that the elements without the SiO_2 passivation layer are much noisier than the SiO_2 passivation treated element. One theory as to why, is the SiO_2 passivation layer is giving a higher thermal resistance between the measurement fluid and the element. This increased thermal resistance acts as a thermal low pass filter for the system, and small non-linearities in the cooling of the element affect the SiO_2 passivation coated element less.

4.4.4 Discussion

The results show a functional flow sensor that is integrated into a standard CMOS process; however, we are severely limited by the small temperature changes of the flow sensor. This causes the need for a high amount of heating current for each element and operating at a higher over heat temperature. The low dynamic range also reduces the accuracy of the system as which must operate close to the comparator's offset. Future design and testing will work to achieve three goals: increase the accuracy of the flow sensor, reduce the power consumption, and improved thermal design for lower flow rates, as found in microfluidics. Further thermal analysis of the flow sensor is required to solve all of these issues. Using a multi-physics thermal simulation, an element can be designed to heat with less power and have predictable response to different flow conditions. A new resistance measurement scheme can replace the current version to provide more dynamic range in our modulator.

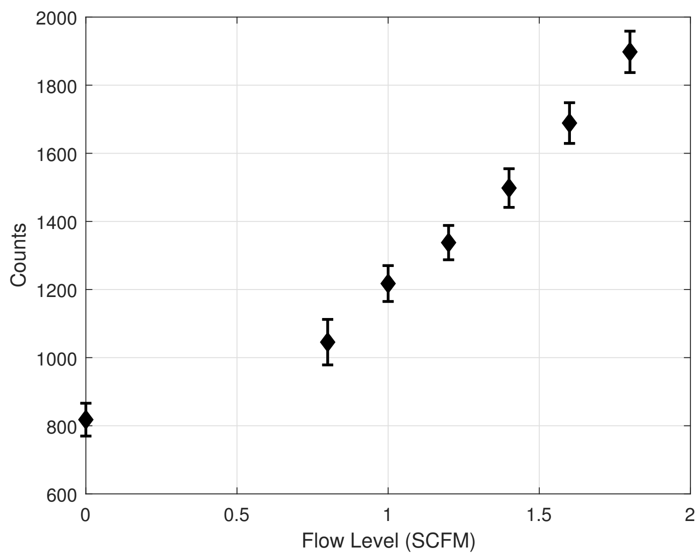

(a)

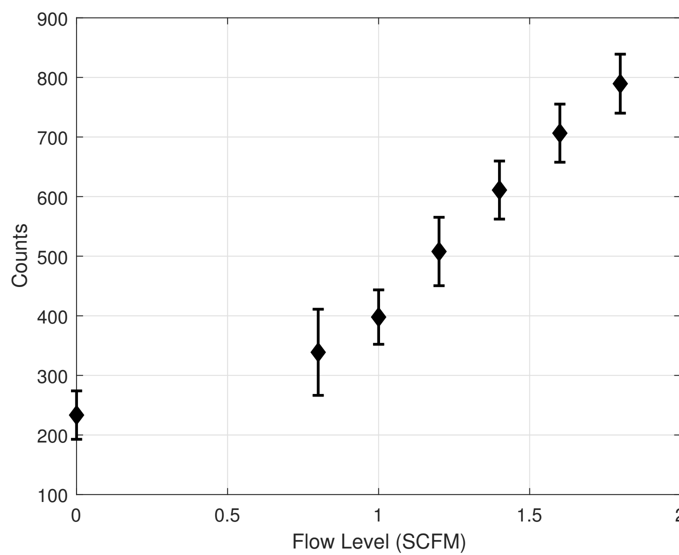

(b)

Figure 4.13: Flow measurement from on-chip element (a) with SiO_2 layer (b) without SiO_2 layer.

Chapter 5: Conclusion and Future Work

5.1 Conclusions

The shrinking of test and control platforms due to advancements in microfluidics manufacturing, MEMS technologies, and the advancement of CMOS has let to an increased demand for smaller highly integrated flow sensing technologies. The shrinking of the sensing platforms are pushing flow sensors to be more sensitive to lower flow values and for flow sensors to operate and process signals in-situ. New thermal flow senors are shrinking and becoming more responsive to lower flow rates, but the need to for multiple sensing elements limits flow sensors integration and manufacturing ability. This work presented a new flow sensing architecture featuring a single element with the goal of providing a simpler and highly integrated thermal flow sensor.

The single-element thermal flow sensor architecture is first demonstrated with a discrete element and control circuitry. A dual-slope control system was developed to enable flow measurement from a single element. The element was manufactured on an epoxy disk and then tested using a regulated air flow setup. The experiments performed demonstrated both the dual-slope control algorithm and the single-element flow sensor's ability to measure flow.

The single-element architecture was then miniaturized and developed for integration with a CMOS chip without post processing. The element was designed in the top metal layers of the chip giving direct access to the flow conditions. The element made use of vias between the top to metal layers to provide it's resistance. The single-element sensor was used in an on chip delta-sigma thermal modulator for flow measurement and control. The delta-sigma modulator required the design of a comparator and decade current source to enable on chip measurement of the single element. The CMOS flow sensing IC was then tested to characterize the element and demonstrate flow sensing performance in a CMOS-integrated flow sensor. The testing demonstrated the IC's response to flow rates from 0.8 to 1.8 SCFM, showing the ability to fully integrate a thermal flow sensor in a standard CMOS process.

5.2 Future Work

Further work is needed for the flow sensor to improve response for lower flow rates, decrease the power consumption, and integrate the single element flow sensor IC with microfluidics. The element design is the largest source of improvement for the thermal flow sensor. Future work could involve thermal/multi-physics simulation to learn more about and improve the thermal response of the element to heating and to flow. With a better understanding of the element, a new measurement circuitry can be implemented to improve the measurable dynamic range and sensitivity to small temperature changes. Also, with a well understood thermal response, power regulation can be integrated on chip increasing the integration of the thermal flow sensor. Finally, with a new flow sensor IC, the sensor can be integrated with microfluidics running across the top of the flow sensor.

Bibliography

[1] M. Ashauer, H. Glosch, F. Hedrich, N. Hey, H. Sandmaier, and W. Lang. Thermal flow sensor for liquids and gases based on combinations of two principles. *Sensors and Actuators A: Physical*, 73(1):7 – 13, 1999.

[2] A. Baldwin, L. Yu, and E. Meng. An electrochemical impedance-based thermal flow sensor for physiological fluids. *Journal of Microelectromechanical Systems*, 25(6):1015–1024, Dec 2016.

[3] K. Clocker, S. Sengupta, M. Lindsay, and M. L. Johnston. Single-element thermal flow sensor using dual-slope control scheme. In *2017 IEEE SENSORS*, pages 1–3, Oct 2017.

[4] M. Dijkstra, M.J. de Boer, J.W. Berenschot, T.S.J. Lammerink, R.J. Wiegerink, and M. Elwenspoek. Miniaturized thermal flow sensor with planar-integrated sensor structures on semicircular surface channels. *Sensors and Actuators A: Physical*, 143(1):1 – 6, 2008. Micromechanics Section of Sensors and Actuators (SAMM), based on contributions revised from the Technical Digest of the IEEE 20th International Conference on Micro Electro Mechanical Systems (MEMS 2007).

[5] T. Dinh, H. P. Phan, A. Qamar, T. K. Nguyen, P. Woodfield, Y. Zhu, N. T. Nguyen, and D. V. Dao. Environment-friendly wearable thermal flow sensors for noninvasive respiratory monitoring. In *2017 IEEE 30th International Conference on Micro Electro Mechanical Systems (MEMS)*, pages 993–996, Jan 2017.

[6] Christian Hoera, Mirjam M. Skadell, Simon A. Pfeiffer, Maik Pahl, Zhe Shu, Erik Beckert, and Detlev Belder. A chip-integrated highly variable thermal flow rate sensor. *Sensors and Actuators B: Chemical*, 225:42 – 49, 2016.

[7] H. M. Jafari and R. Genov. Cmos impedance spectrum analyzer with dual-slope multiplying adc. In *2011 IEEE Biomedical Circuits and Systems Conference (BioCAS)*, pages 361–364, Nov 2011.

[8] J KIELBASA, J RYSZ, A.Z. SMOLARSKI, and Boleslaw Stasicki. The oscillatory anemometer. 1, 01 1972.

[9] Theo S.J. Lammerink, Fred Dijkstra, Zweitze Houkes, and Joost van Kuijk. Intelligent gas-mixture flow sensor. *Sensors and Actuators A: Physical*, 47(1):380 – 384, 1995.

[10] H. Lee, S. Baek, E. Jeon, and J. Lee. Microneedle thermal flow sensor. In *2016 IEEE SENSORS*, pages 1–3, Oct 2016.

[11] A. De Luca, C. Falco, E. L. W. Gardner, J. D. Coull, and F. Udrea. Diode-based cmos mems thermal flow sensors. In *2017 19th International Conference on Solid-State Sensors, Actuators and Microsystems (TRANSDUCERS)*, pages 2211–2214, June 2017.

[12] K.A.A. Makinwa and J.H. Huijsing. A wind-sensor interface using thermal sigma delta modulation techniques. *Sensors and Actuators A: Physical*, 92(1):280 – 285, 2001. Selected Papers for Eurosensors XIV.

[13] M. Mullins, R. Bayford, A. Van Putten, and J. Butcher. Design and fabrication of single-chip intelligent silicon thermal flow sensors in standard cmos technology. In *IEE Colloquium on Advances in Sensors for Fluid Flow Measurement*, pages 14/1–14/4, Apr 1996.

[14] A. J. Mki, A. Kontunen, T. Ryynnen, J. Verho, J. Kreutzer, J. Lekkala, and P. Kallio. Design and simulation of a thermal flow sensor for gravity-driven microfluidic applications. In *2016 IEEE 11th Annual International Conference on Nano/Micro Engineered and Molecular Systems (NEMS)*, pages 125–129, April 2016.

[15] Bas Oudheusden. Silicon thermal flow sensors. 30:5–26, 01 1992.

[16] H. Ouh, S. Sengupta, S. Bose, and M. L. Johnston. Dual-mode, enhanced dynamic range cmos optical sensor for biomedical applications. In *2017 IEEE Biomedical Circuits and Systems Conference (BioCAS)*, pages 1–4, Oct 2017.

[17] Jian-Bo Sun, Ming Qin, and Qing-An Huang. A flip-chip packaged cmos thermal flow sensor. In *IEEE Sensors, 2005.*, pages 4 pp.–, Oct 2005.

[18] Jianhai Sun, Dafu Cui, Lulu Zhang, Xing Chen, Haoyuan Cai, and Hui Li. Fabrication and characterization of a double-heater based mems thermal flow sensor. *Sensors and Actuators A: Physical*, 193:25 – 29, 2013.

[19] O. Tabata. Fast-response silicon flow sensor with an on-chip fluid temperature sensing element. *IEEE Transactions on Electron Devices*, 33(3):361–365, Mar 1986.

[20] A.F.P. van Putten. An integrated silicon double bridge anemometer. *Sensors and Actuators*, 4:387 – 396, 1983.

[21] H. J. Verhoeven and J. H. Huijsing. Design of thermal sigma-delta modulators for smart thermal sensors. In *Circuits and Systems, 1995. ISCAS '95., 1995 IEEE International Symposium on*, volume 1, pages 179–182 vol.1, Apr 1995.

[22] Huibert-Jan Verhoeven and Johan H. Huijsing. Design of integrated thermal flow sensors using thermal sigmadelta modulation. *Sensors and Actuators A: Physical*, 52(1):198 – 202, 1996. Proceedings of the 8th International Conference on Solid-State Sensors and Actuators Eurosensors IX.

[23] Chun-Hui Wu, Dongyang Kang, Ping-Hei Chen, and Yu-Chong Tai. Mems thermal flow sensors. *Sensors and Actuators A: Physical*, 241:135 – 144, 2016.

[24] W. Xu, B. Gao, M. Ahmed, M. Duan, B. Wang, S. Mohamad, A. Bermak, and Y. K. Lee. A wafer-level encapsulated cmos mems thermoresistive calorimetric flow sensor with integrated packaging design. In *2017 IEEE 30th International Conference on Micro Electro Mechanical Systems (MEMS)*, pages 989–992, Jan 2017.